Supporting Information

Easier to Twist than Bend: The Scope of the Bridge Formation Approach to Naphthalenophane Synthesis

Anjan Bedi,[a]* Linda J. W. Shimon,[b] Benny Bogoslavsky,[a] and Ori Gidron [a]*

[a]Institute of Chemistry, The Hebrew University of Jerusalem, Edmond J. Safra Campus, Jerusalem, Israel. [b]Chemical Research Support Unit, Weizmann Institute of Science, Rehovot, Israel.

Contents

S1 Characterization

S1.1 Characterization of compound 3

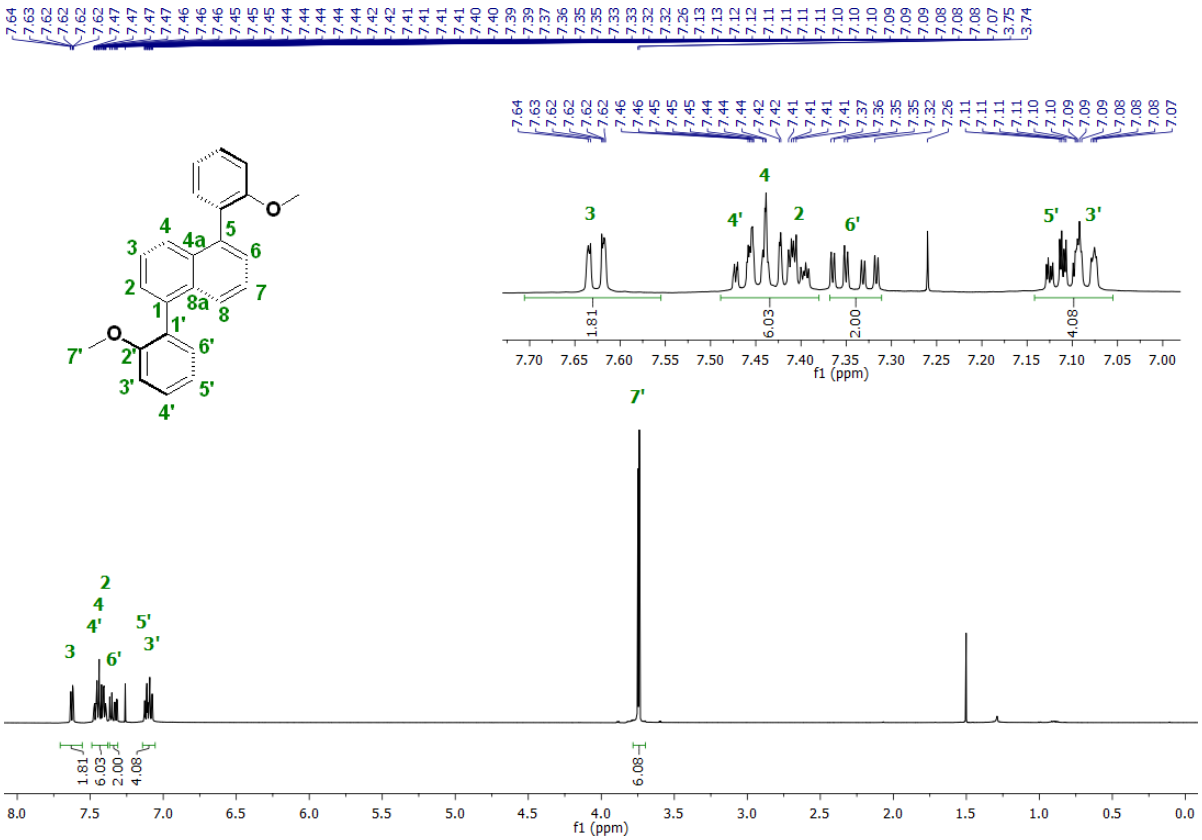

Figure S1. ^{1}H NMR of compound **3** in $CDCl_3$ at 298 K.

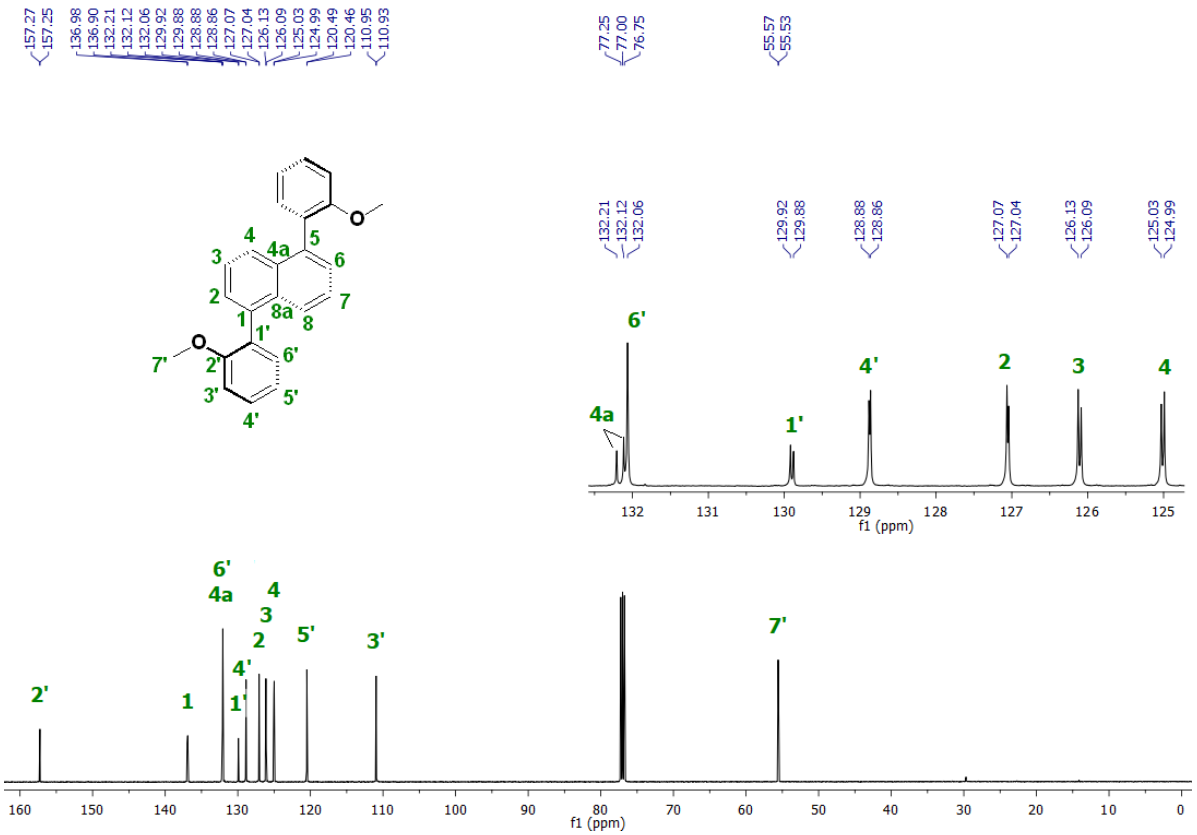

Figure S2. ^{13}C NMR of compound **3** in $CDCl_3$ at 298 K.

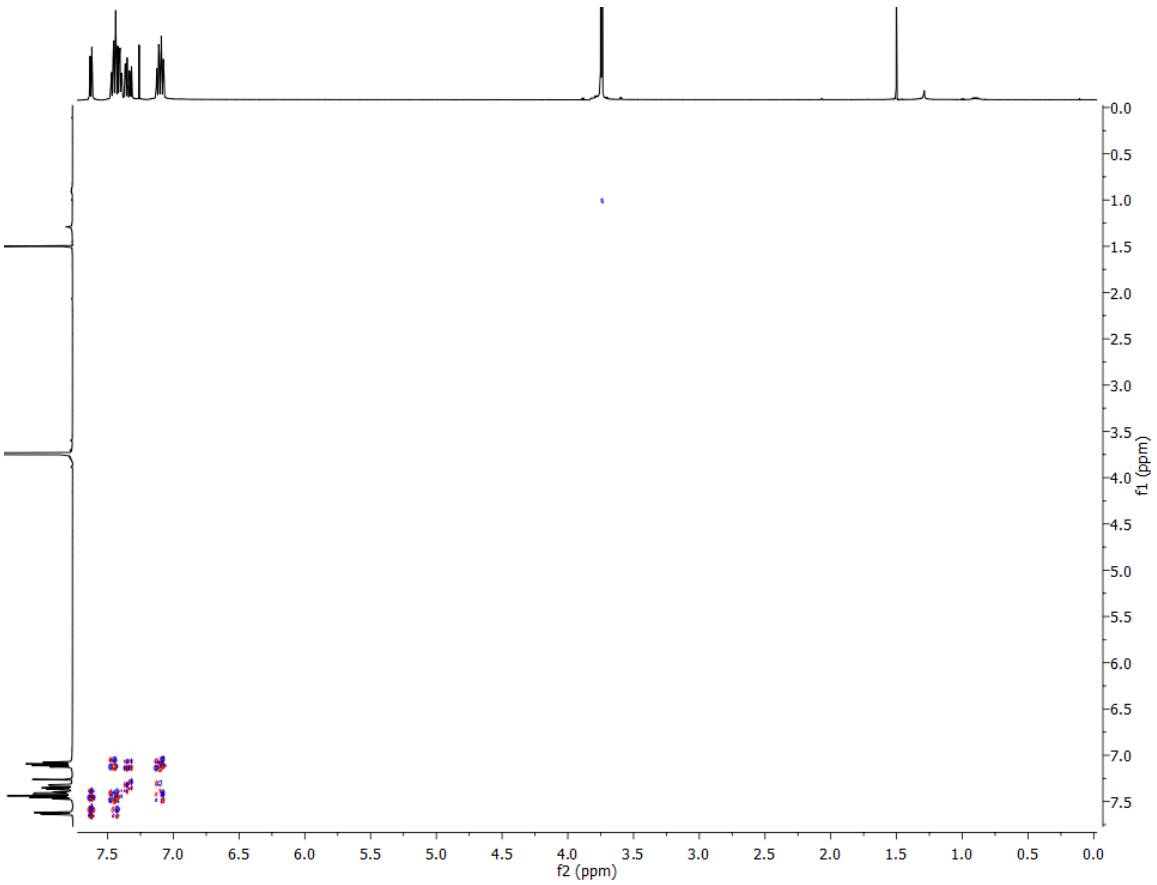

Figure S3. COSY NMR of compound **3** in $CDCl_3$ at 298 K.

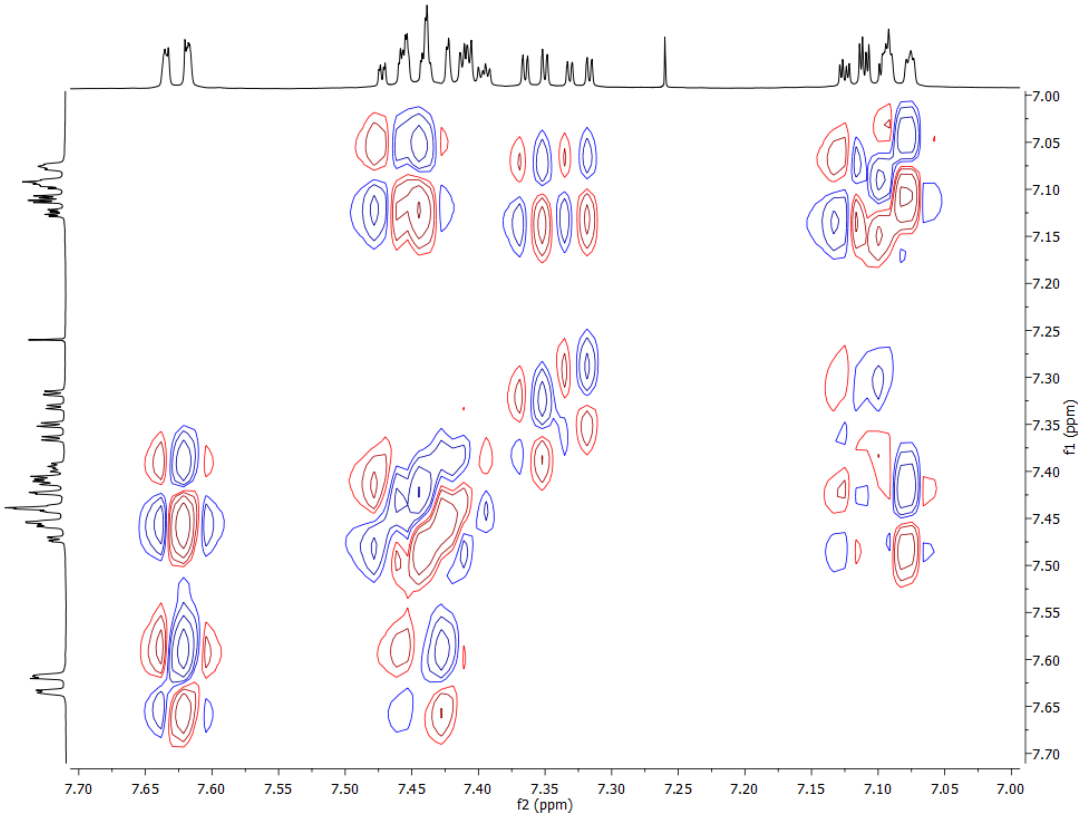

Figure S4. COSY NMR of compound **3** in $CDCl_3$ at 298 K. Expansion of the aromatic region.

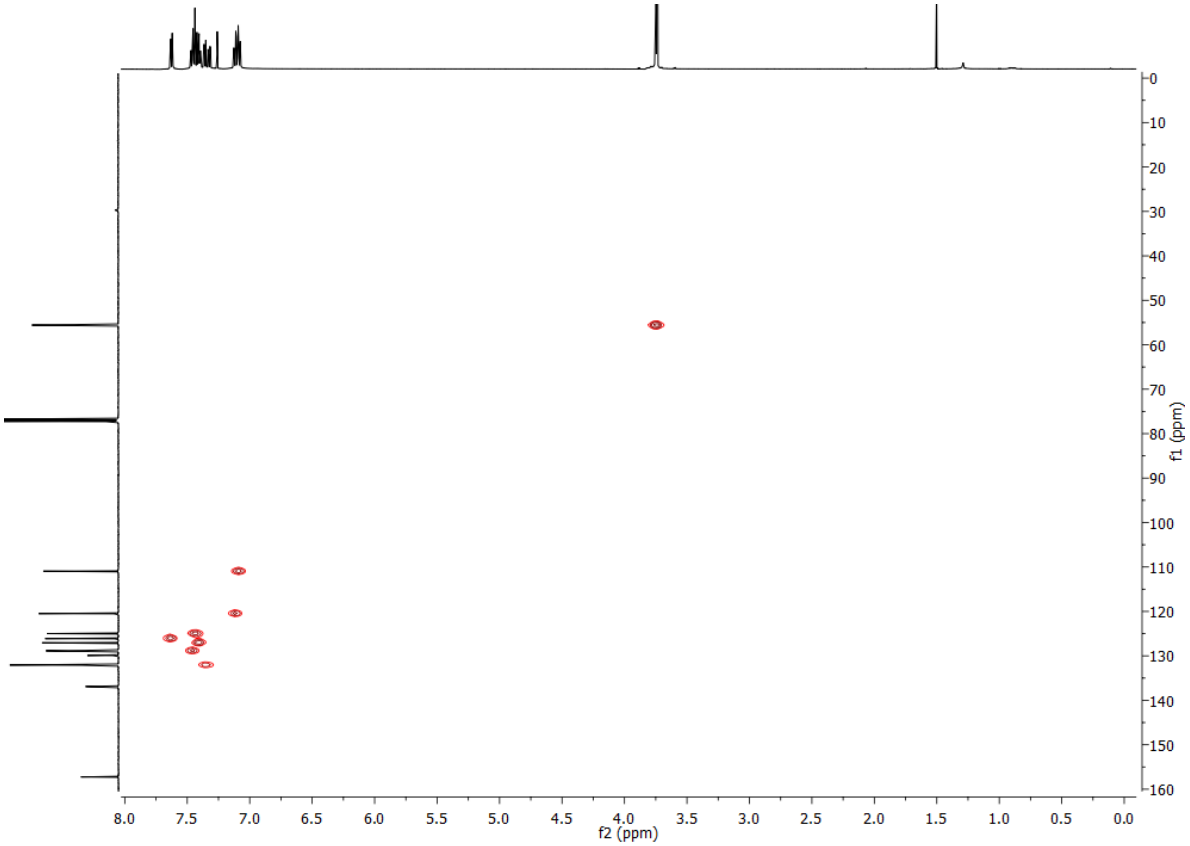

Figure S5. HSQC NMR of compound **3** in $CDCl_3$ at 298 K.

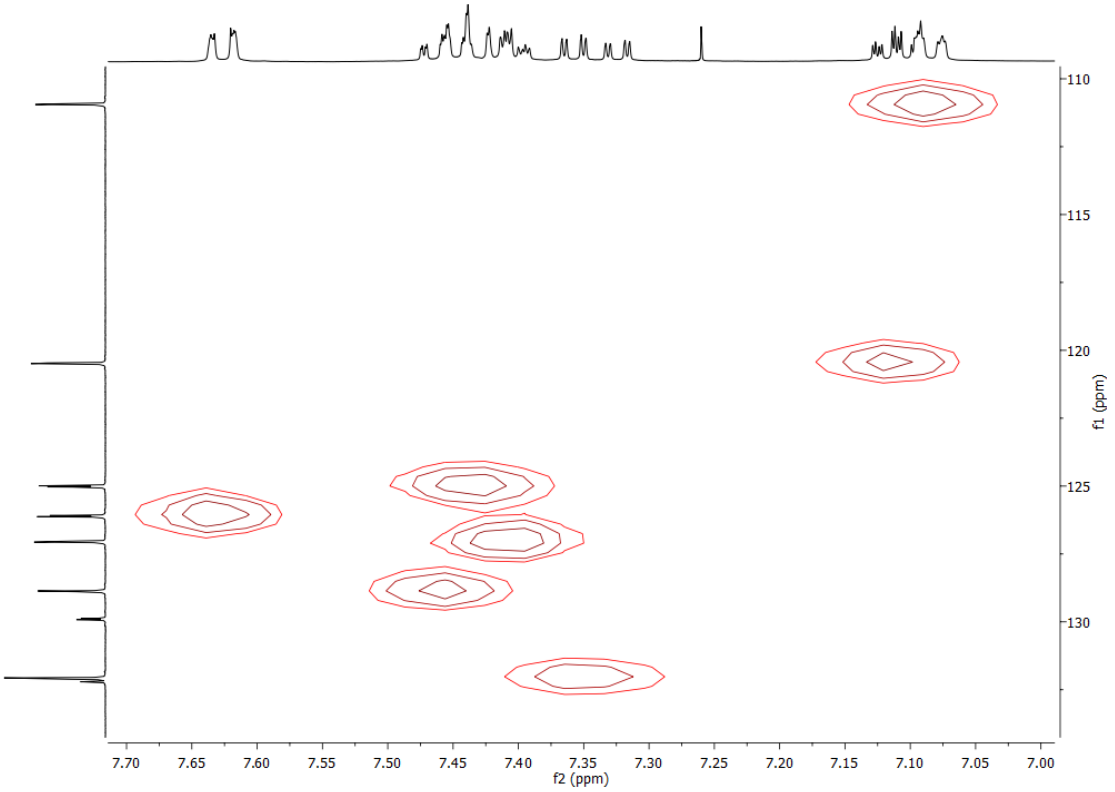

Figure S6. HSQC NMR of compound **3** in $CDCl_3$ at 298 K. Expansion of the aromatic region.

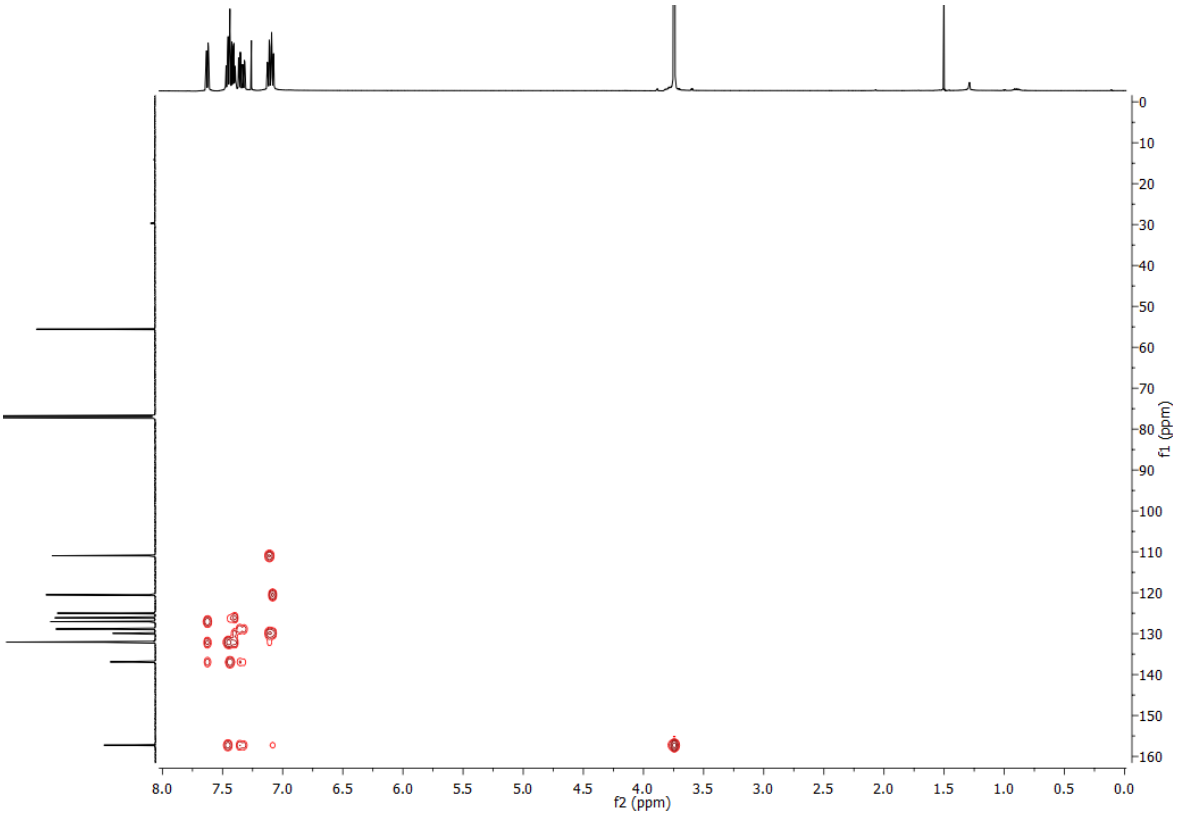

Figure S7. HMBC NMR of compound **3** in $CDCl_3$ at 298 K

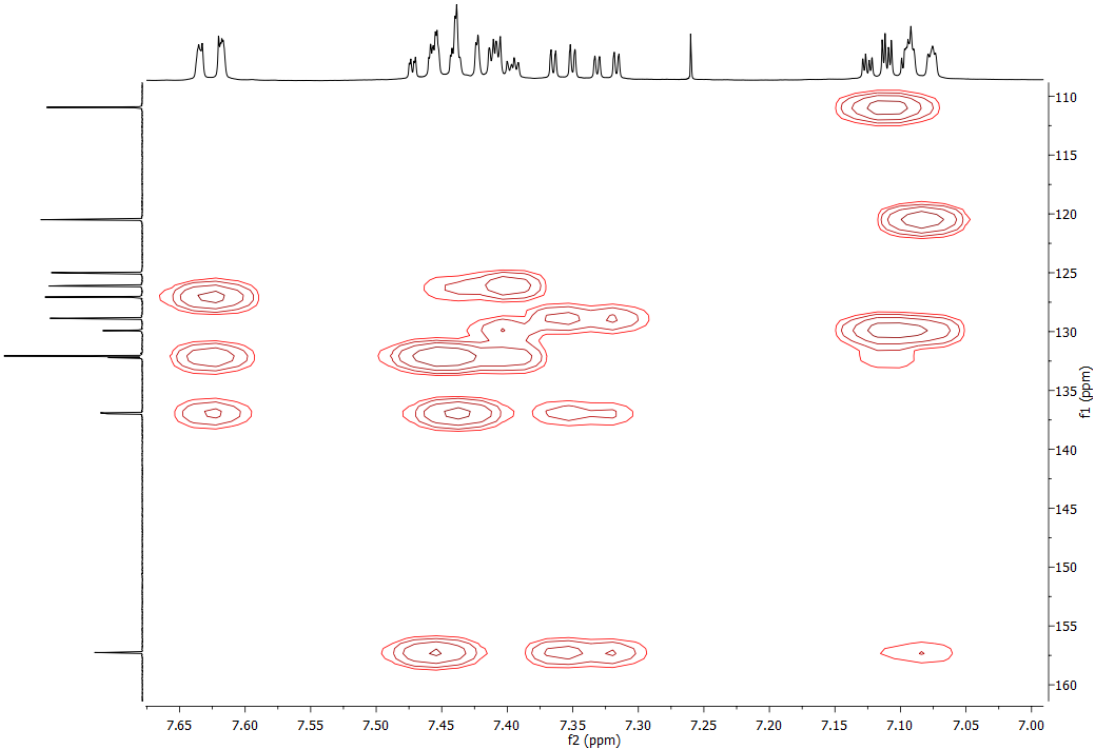

Figure S8. HMBC NMR of compound **3** in $CDCl_3$ at 298 K. Expansion of the aromatic region.

S1.2 Characterization of compound 4

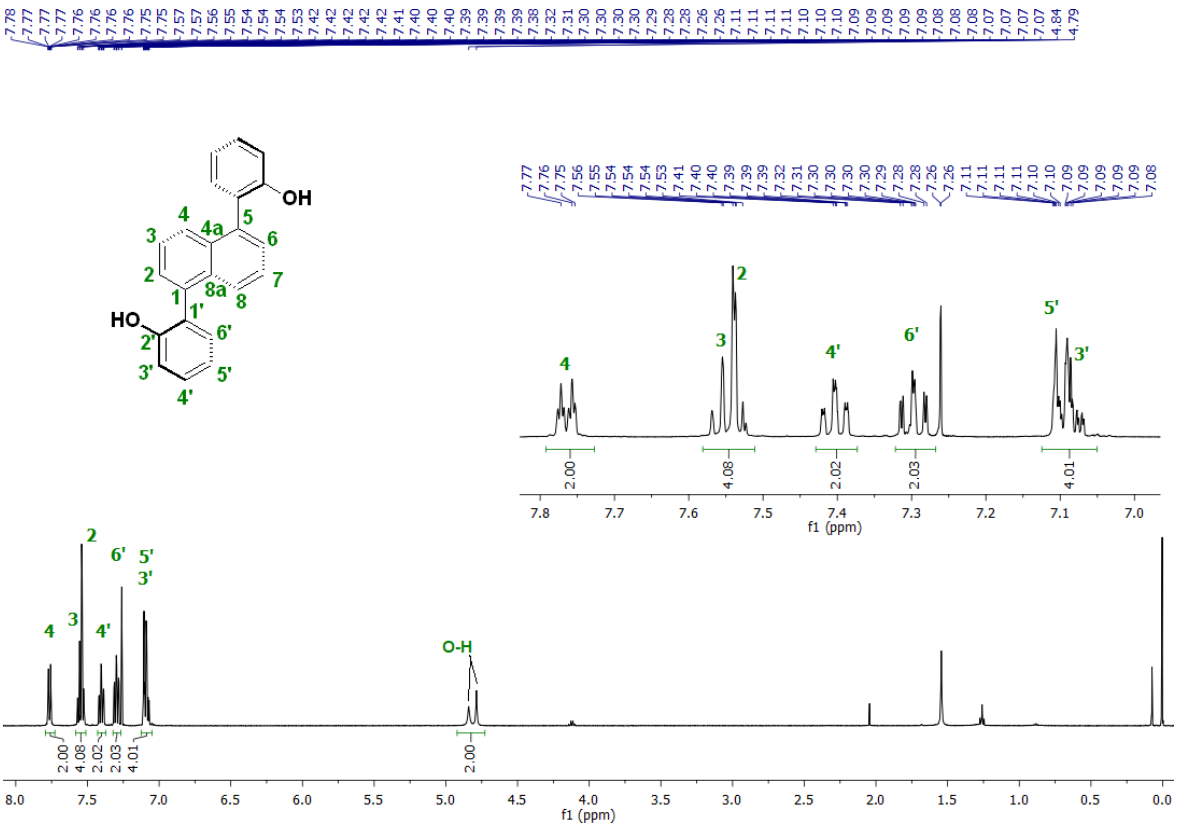

Figure S9. ^1H NMR of compound **4** in $CDCl_3$ at 298 K.

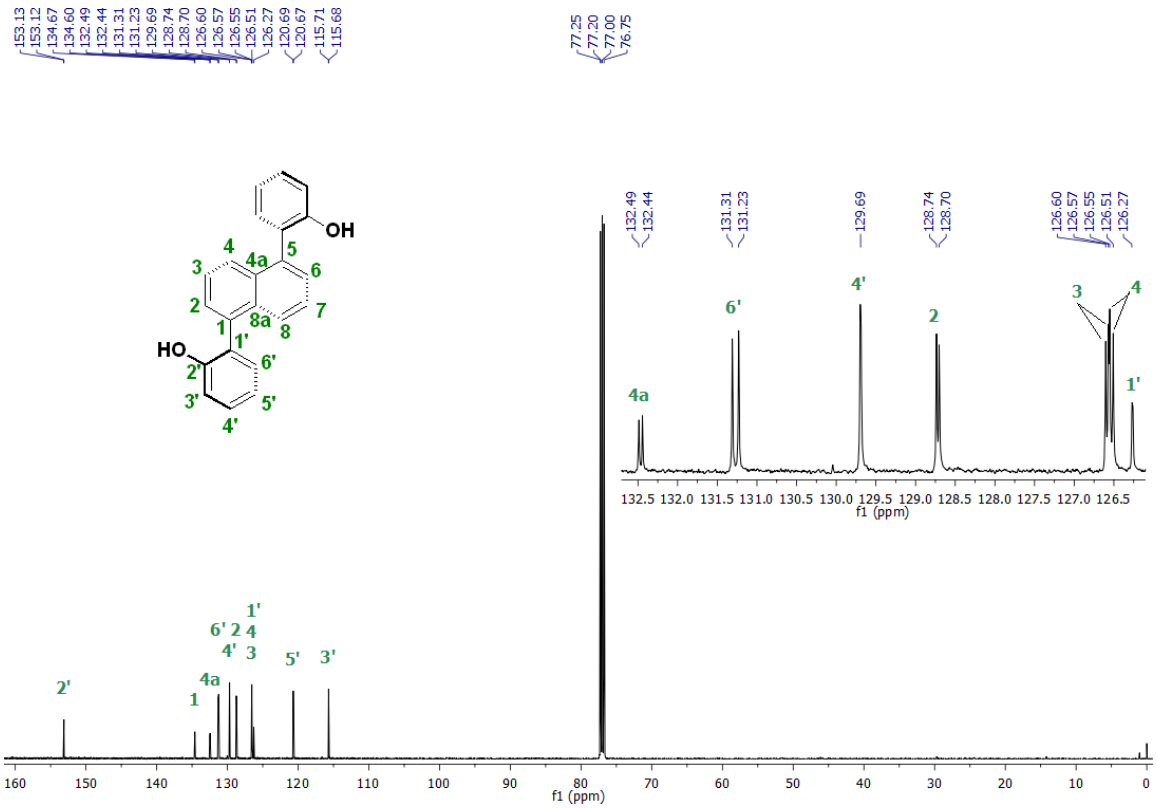

Figure S10. ^{13}C NMR of compound **4** in $CDCl_3$ at 298 K.

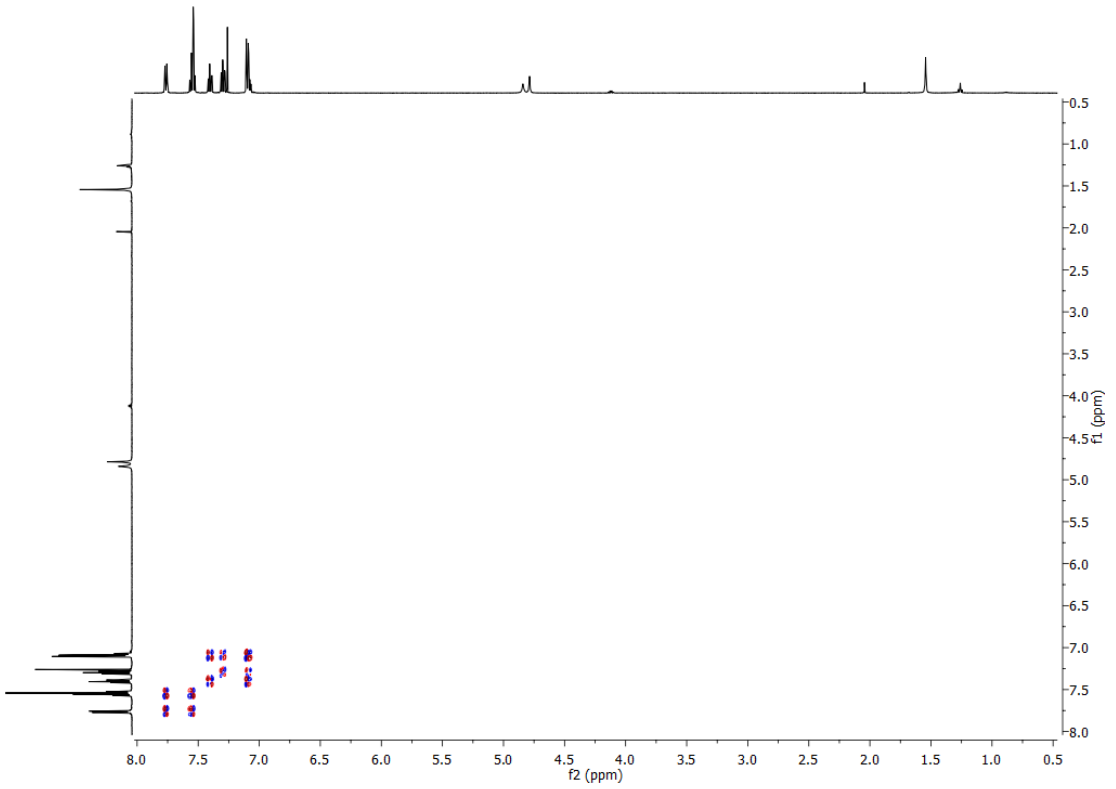

Figure S11. COSY NMR of compound **4** in $CDCl_3$ at 298 K.

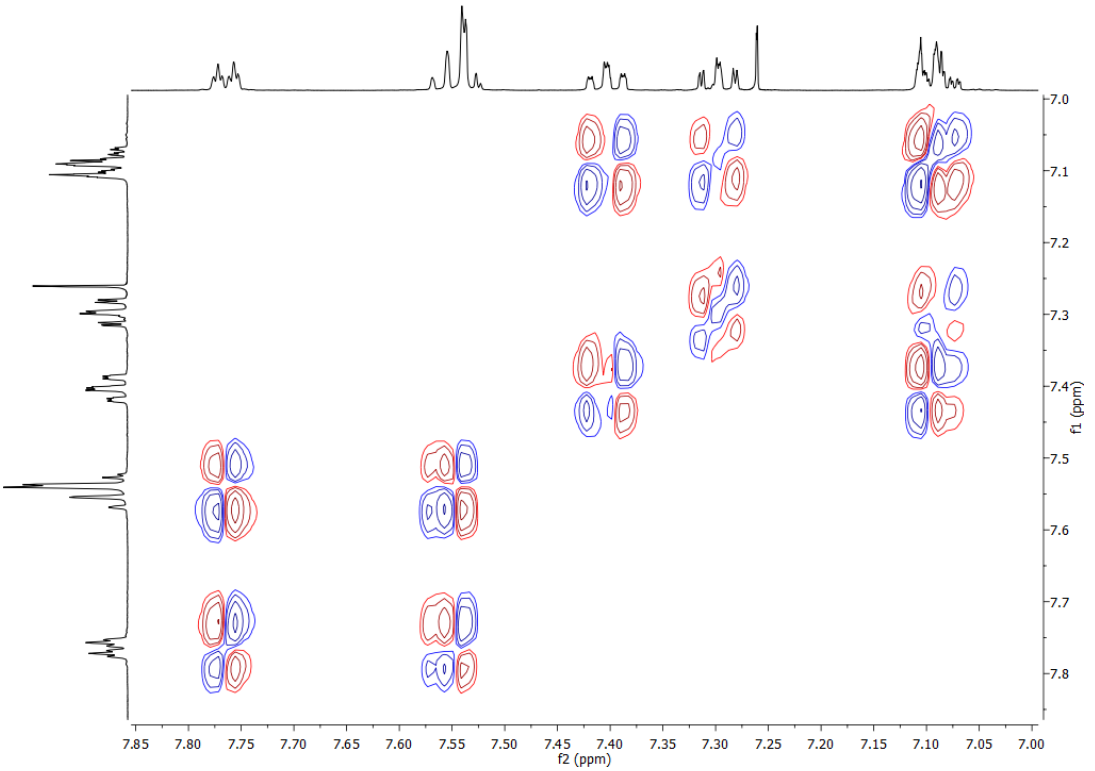

Figure 12. COSY NMR of compound **4** in $CDCl_3$ at 298 K. Expansion of the aromatic region.

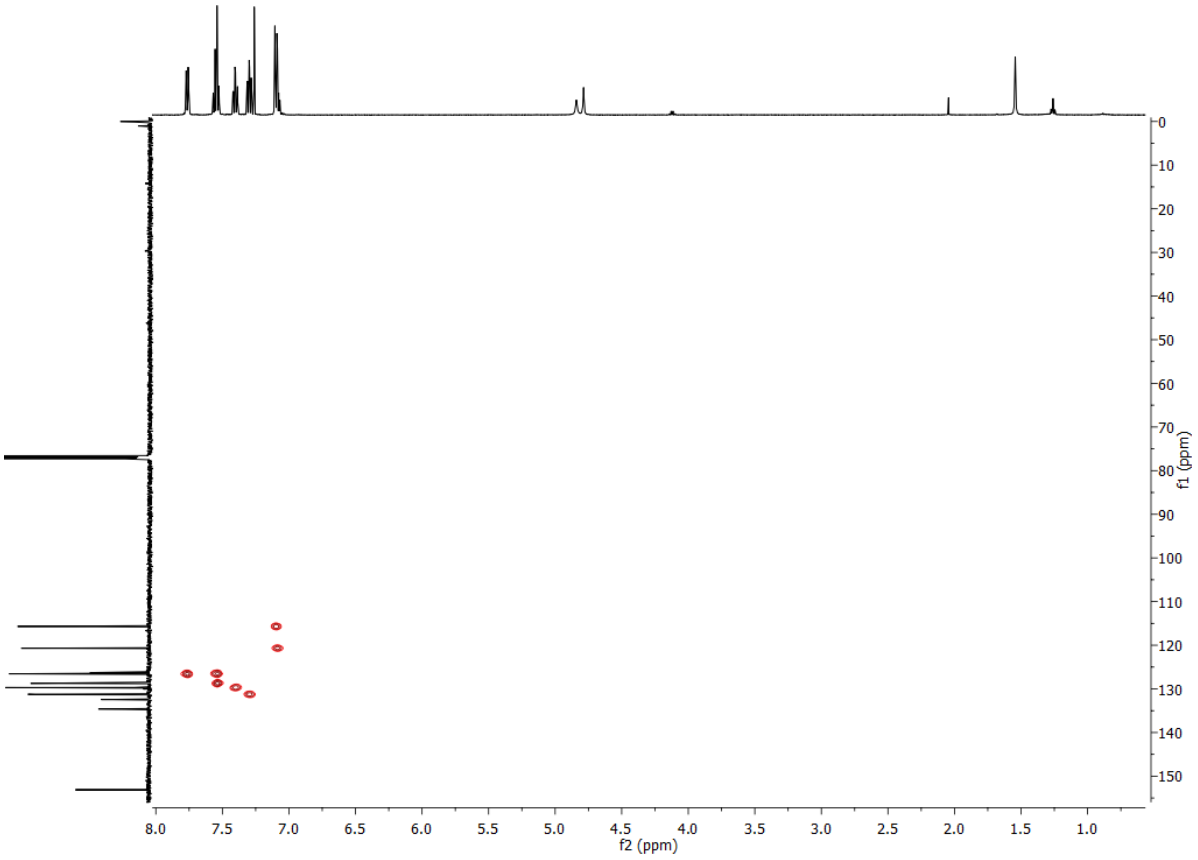

Figure S13. HSQC NMR of compound **4** in $CDCl_3$ at 298 K.

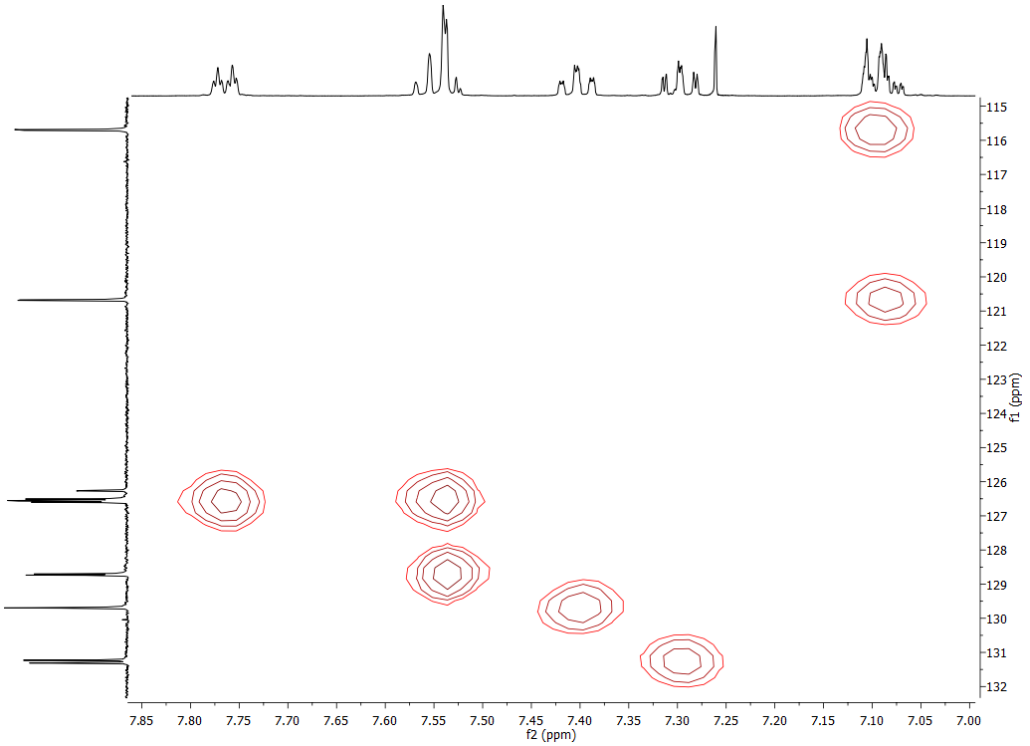

Figure S14. HSQC NMR of compound **4** in $CDCl_3$ at 298 K. Expansion of the aromatic region.

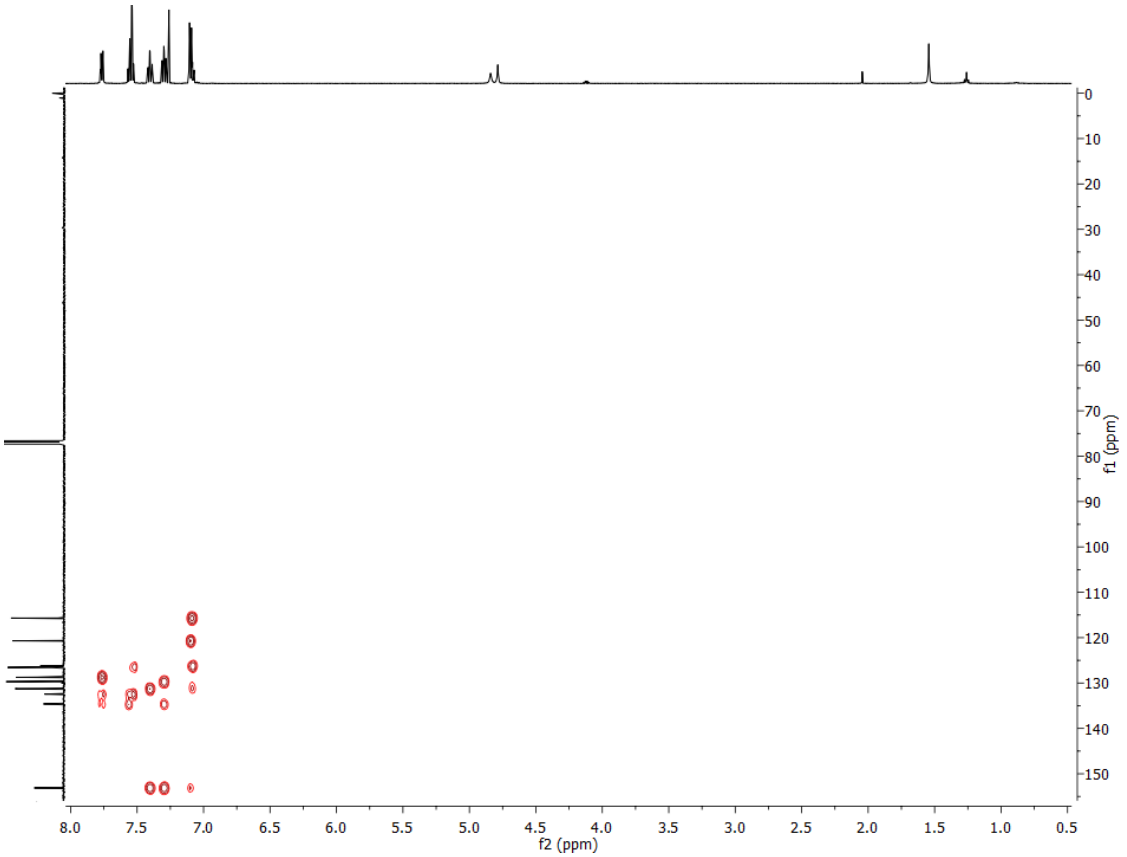

Figure S15. HMBC NMR of compound **4** in $CDCl_3$ at 298 K.

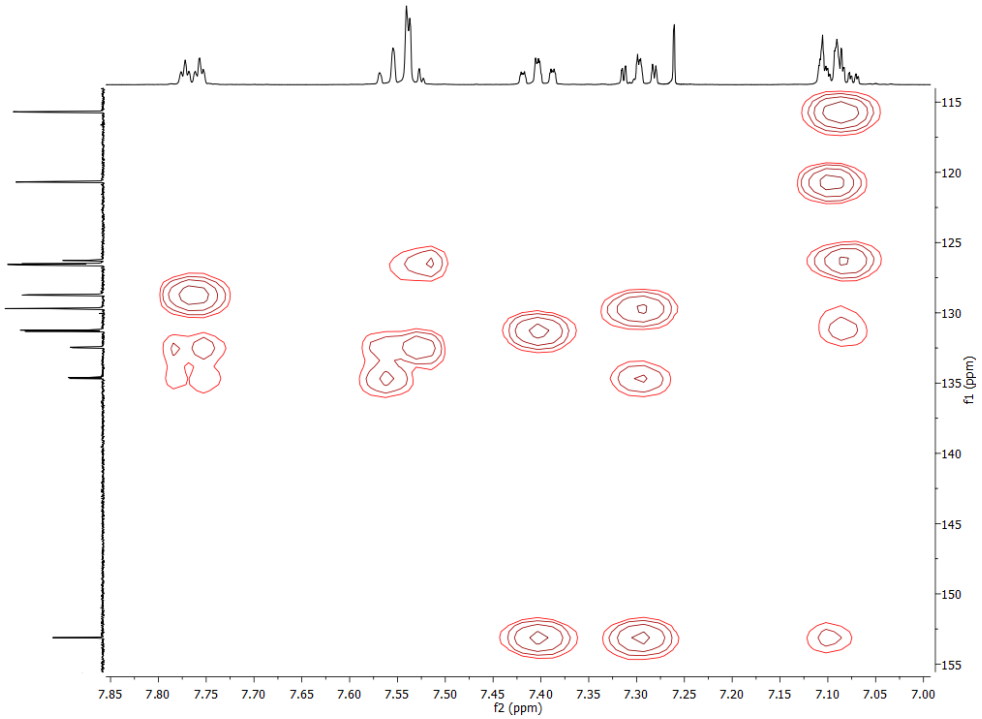

Figure S16. HMBC NMR of compound **4** in $CDCl_3$ at 298 K. Expansion of the aromatic region.

S1.3 Characterization of Nap-C6

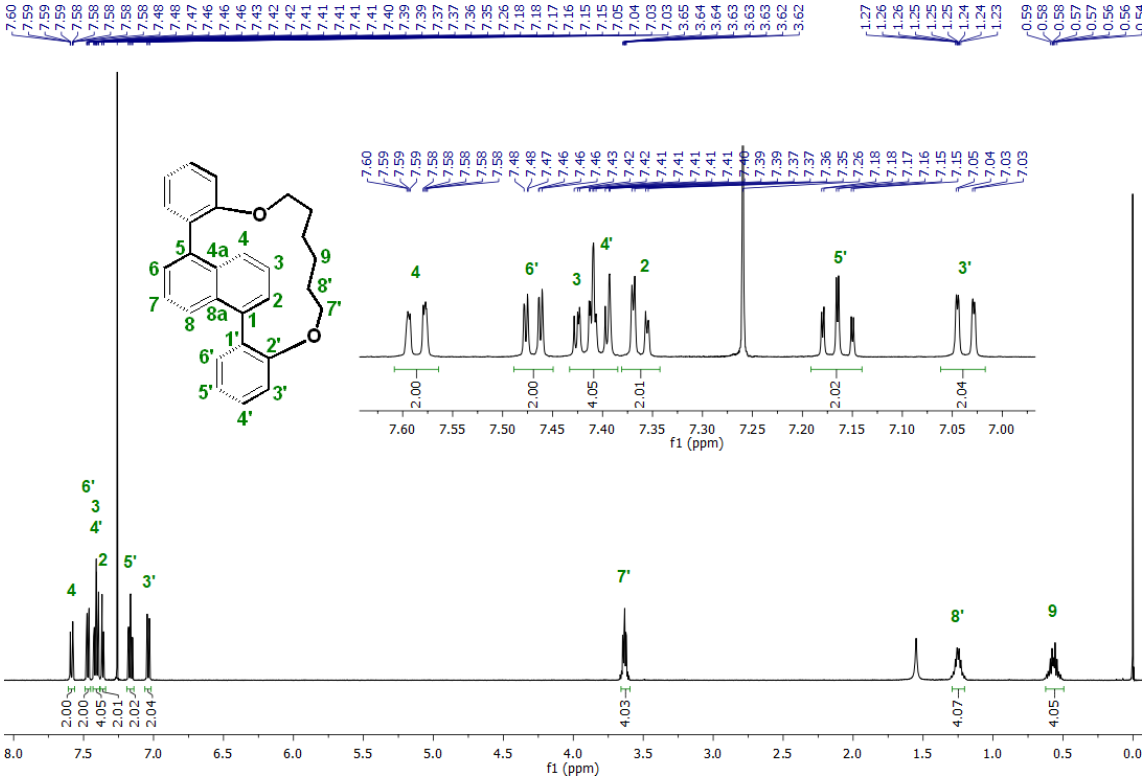

Figure S17. ^{1}H NMR of **Nap-C6** in $CDCl_3$ at 298 K.

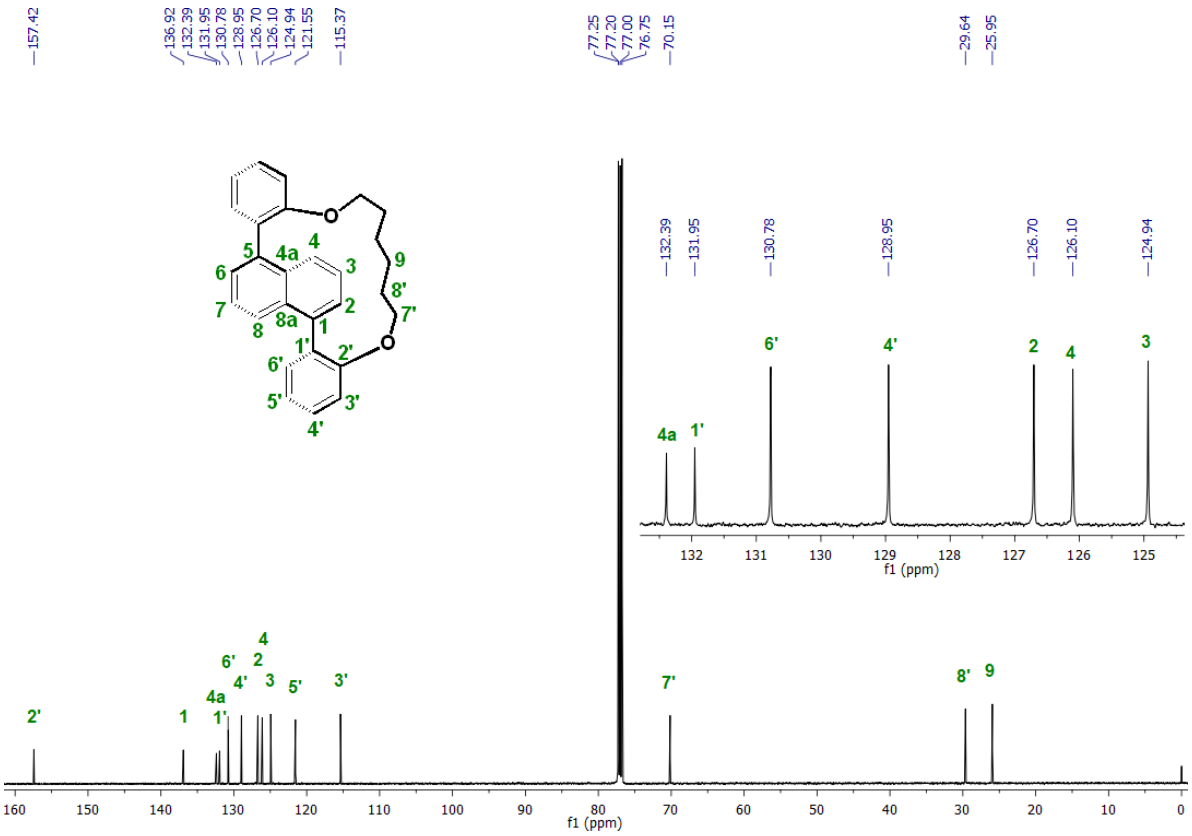

Figure S18. ^{13}C NMR of **Nap-C6** in $CDCl_3$ at 298 K.

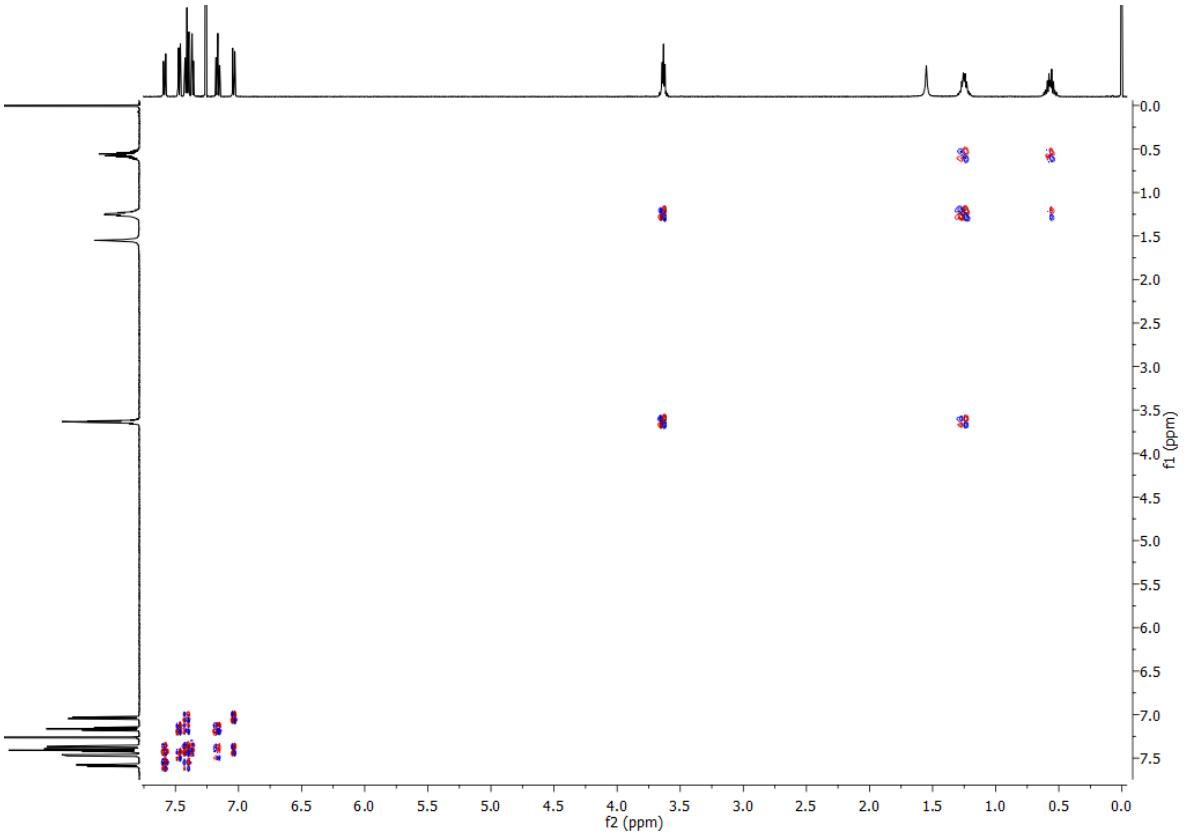

Figure S19. COSY NMR of **Nap-C6** in $CDCl_3$ at 298 K.

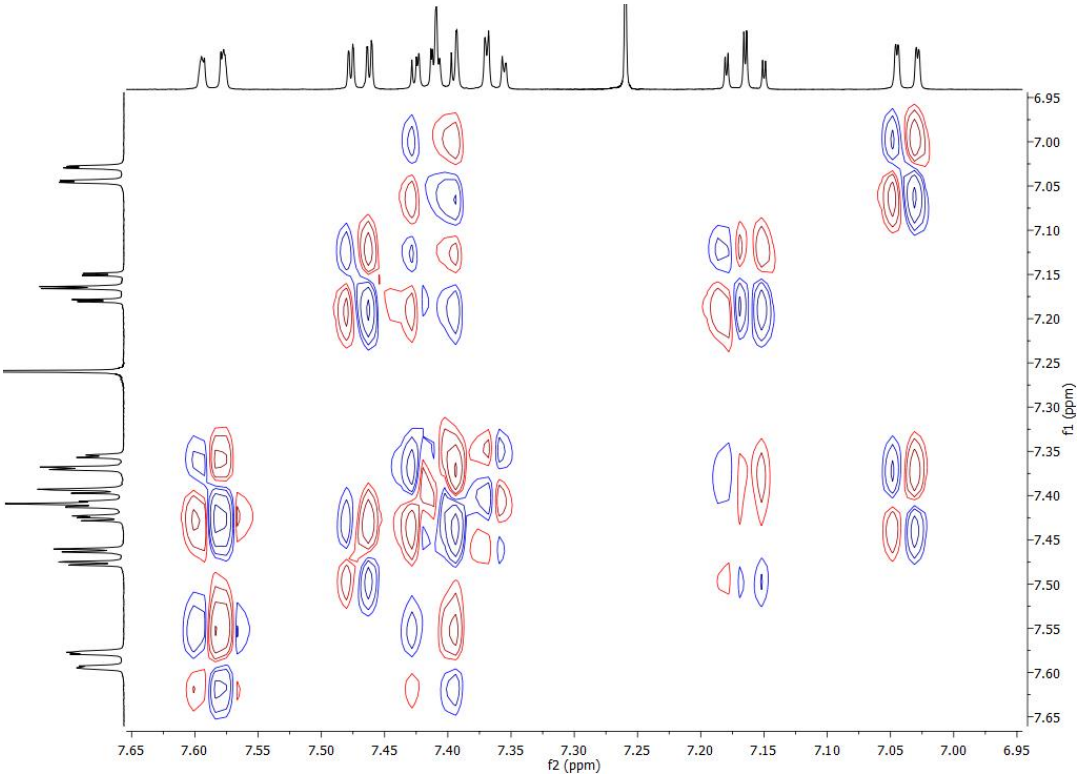

Figure S20. COSY NMR of **Nap-C6** in $CDCl_3$ at 298 K. Expansion of the aromatic region.

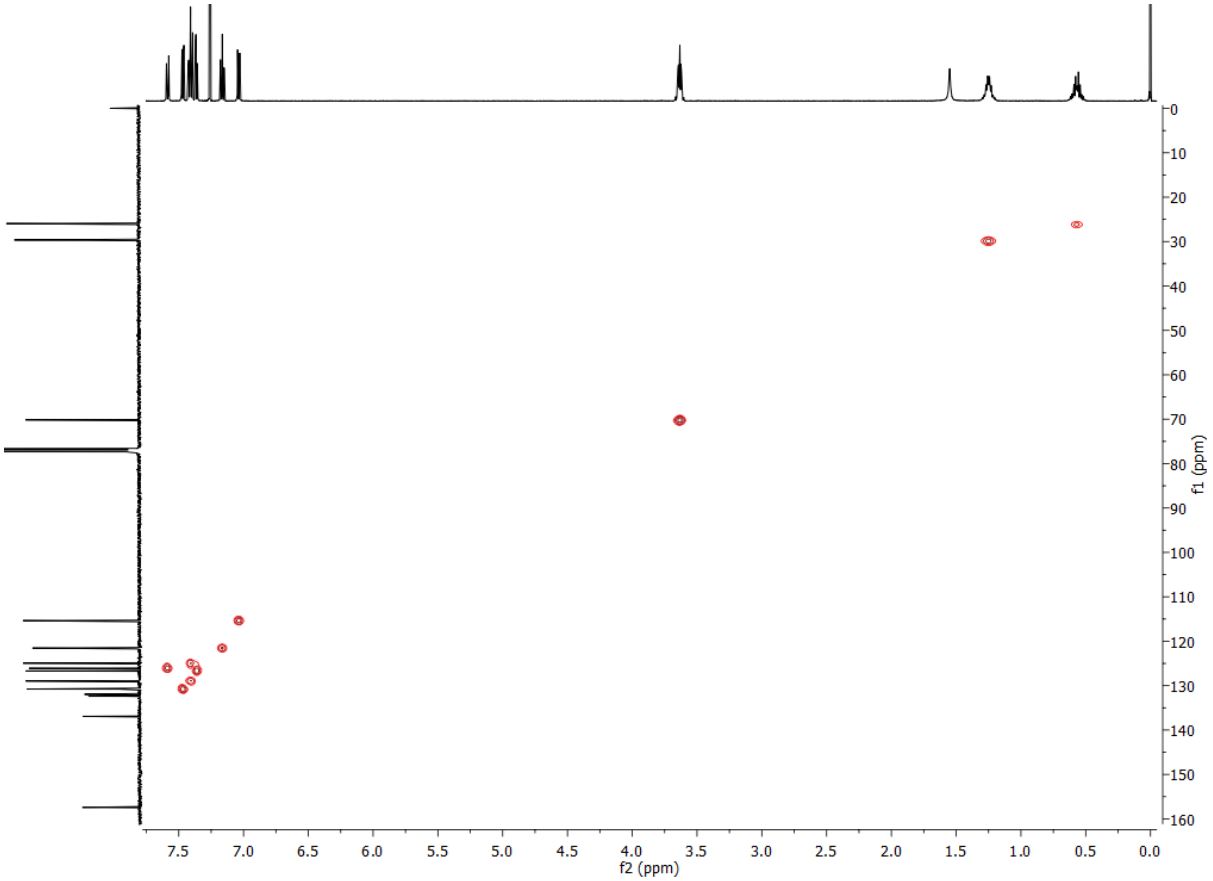

Figure S21. HSQC NMR of **Nap-C6** in $CDCl_3$ at 298 K.

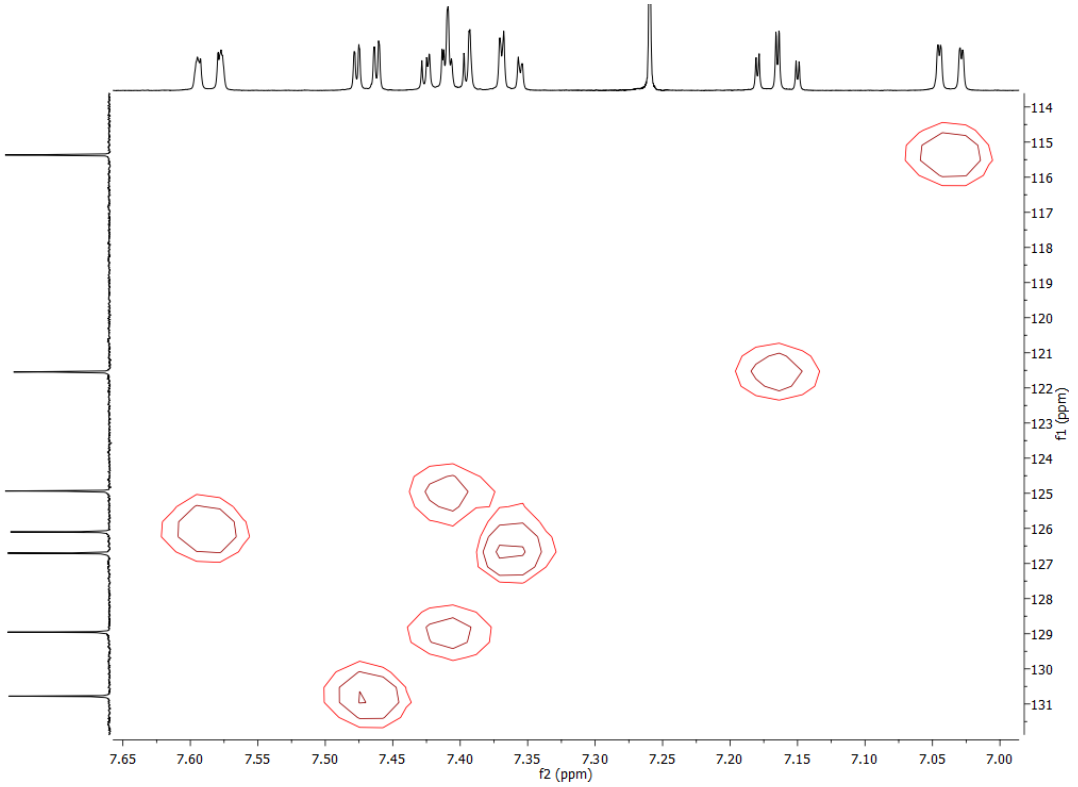

Figure S22. HSQC NMR of **Nap-C6** in $CDCl_3$ at 298 K. Expansion of the aromatic region.

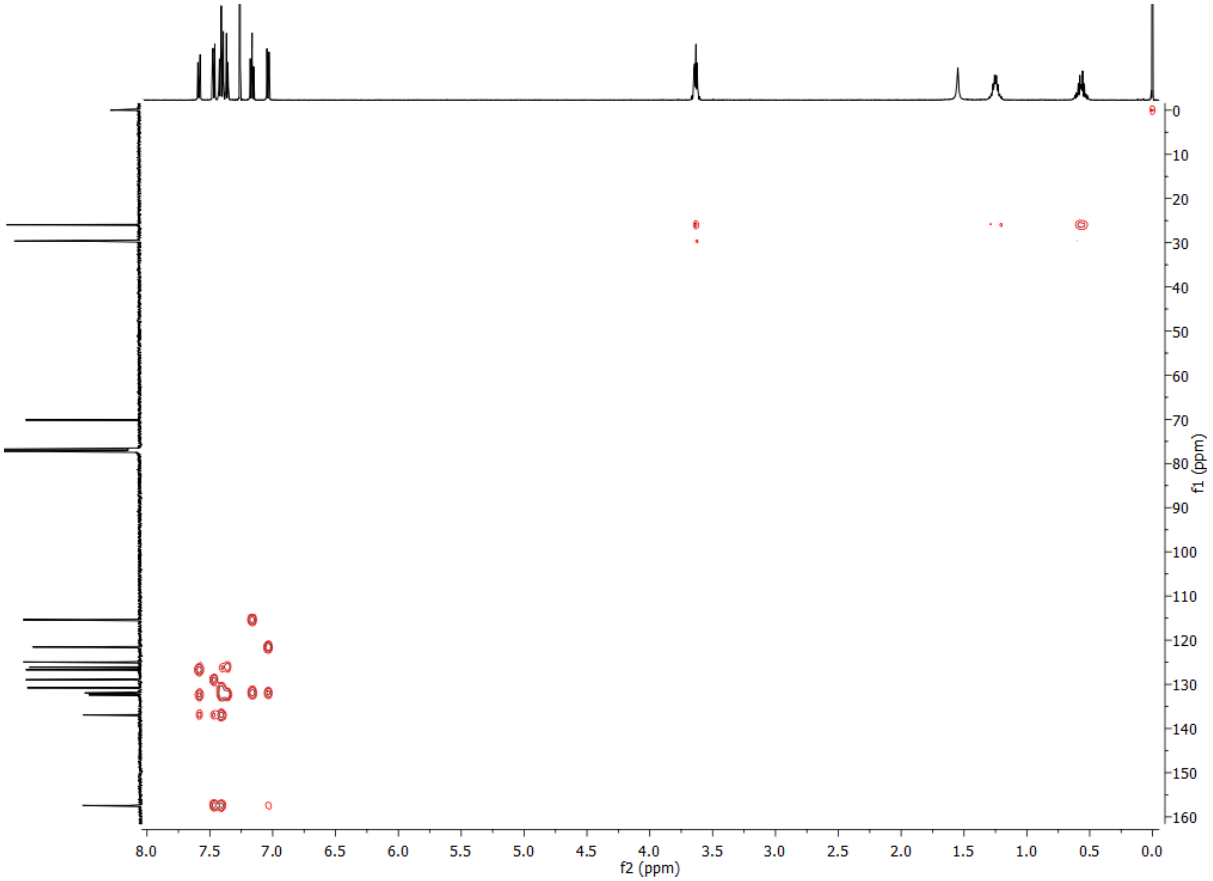

Figure S23. HMBC NMR of **Nap-C6** in $CDCl_3$ at 298 K.

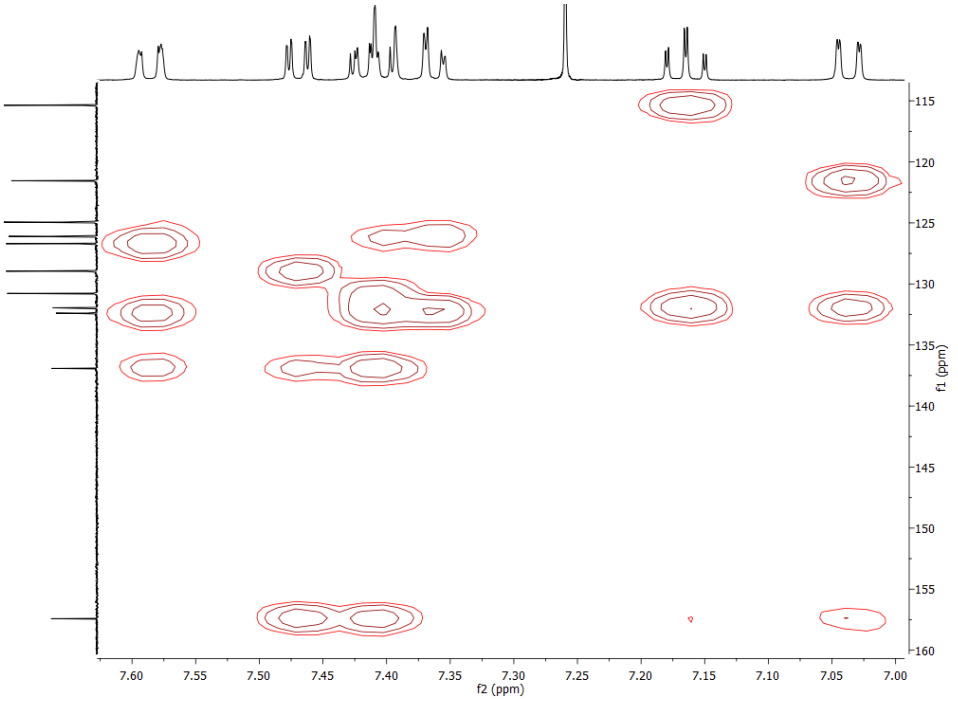

Figure S24. HMBC NMR of **Nap-C6** in $CDCl_3$ at 298 K. Expansion of the aromatic region.

S1.4 Characterization of Nap-C4

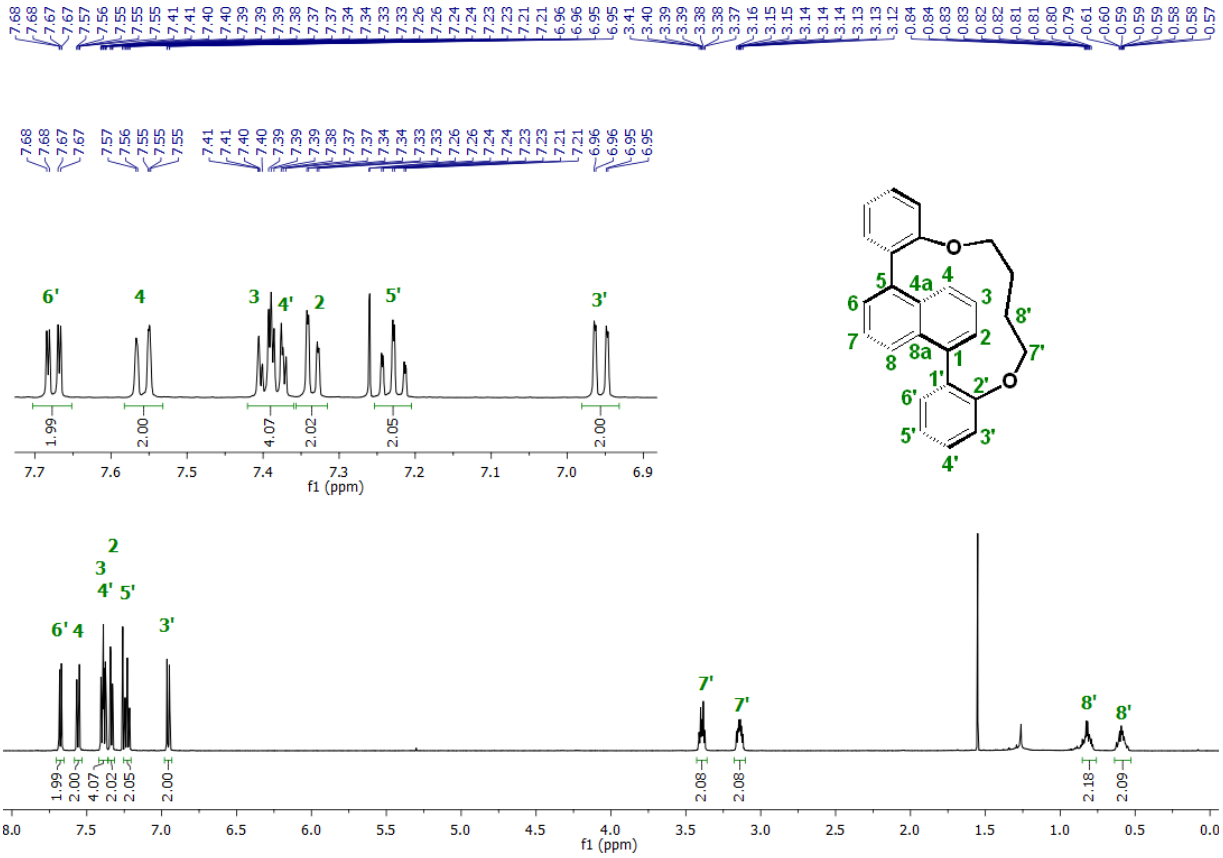

Figure 25. ^1H NMR of **Nap-C4** in $CDCl_3$ at 298 K.

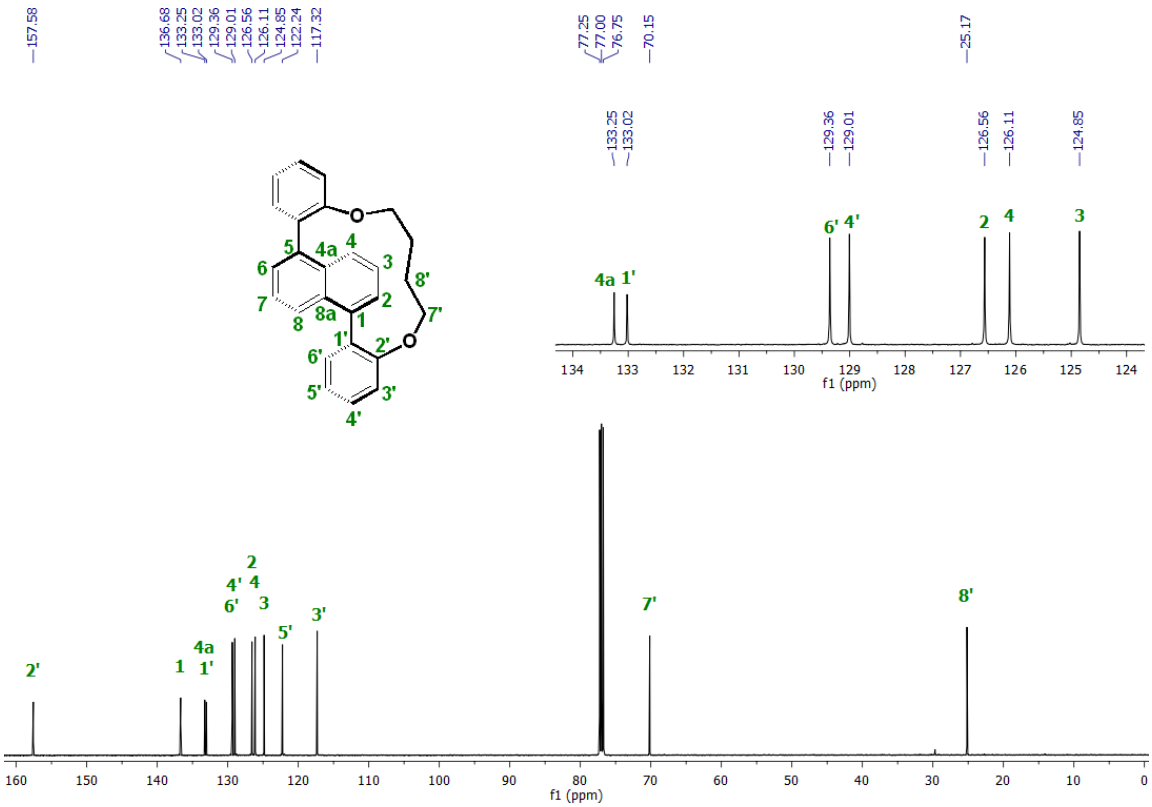

Figure S26. ^{13}C NMR of **Nap-C4** in $CDCl_3$ at 298 K.

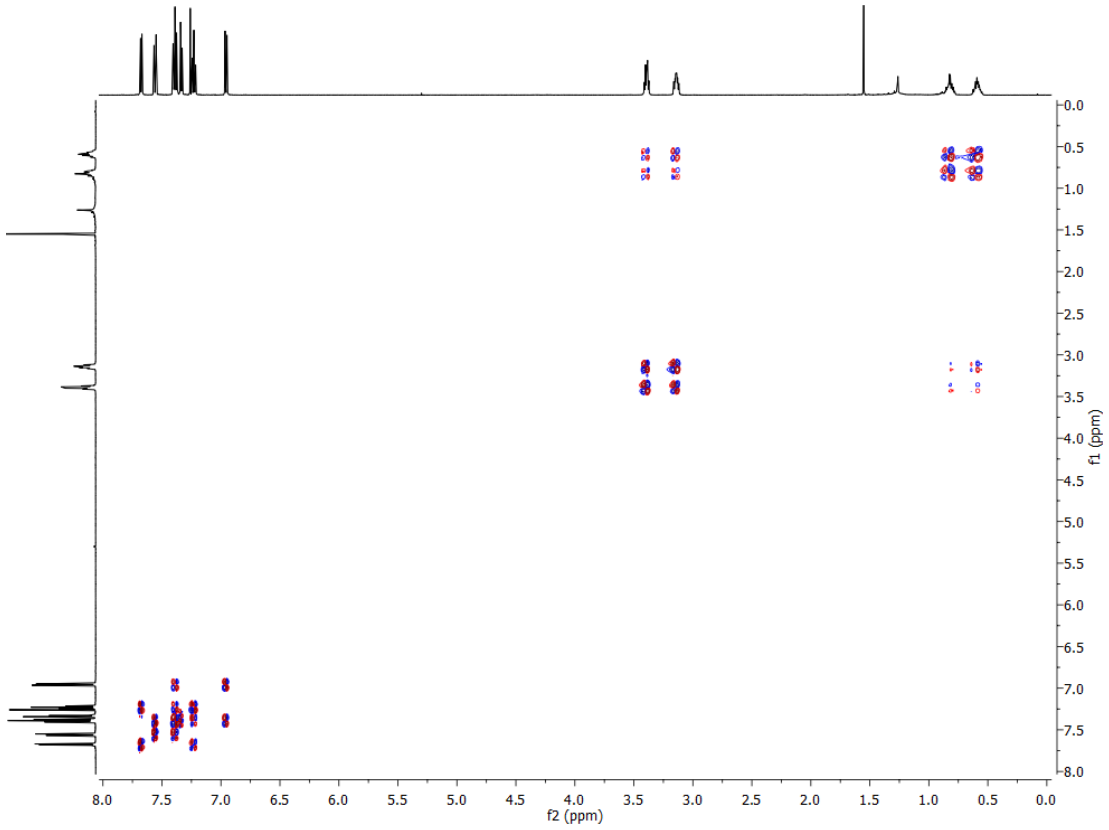

Figure S27. COSY NMR of **Nap-C4** in $CDCl_3$ at 298 K.

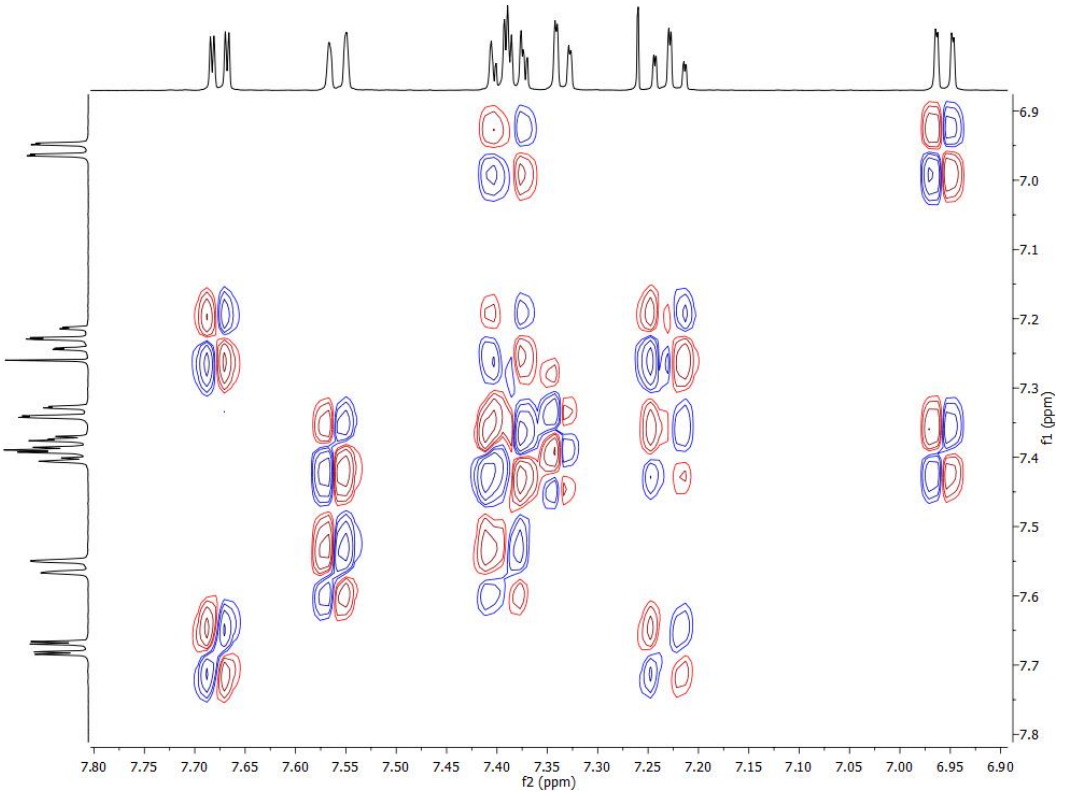

Figure S28. COSY NMR of **Nap-C4** in $CDCl_3$ at 298 K. Expansion of the aromatic region.

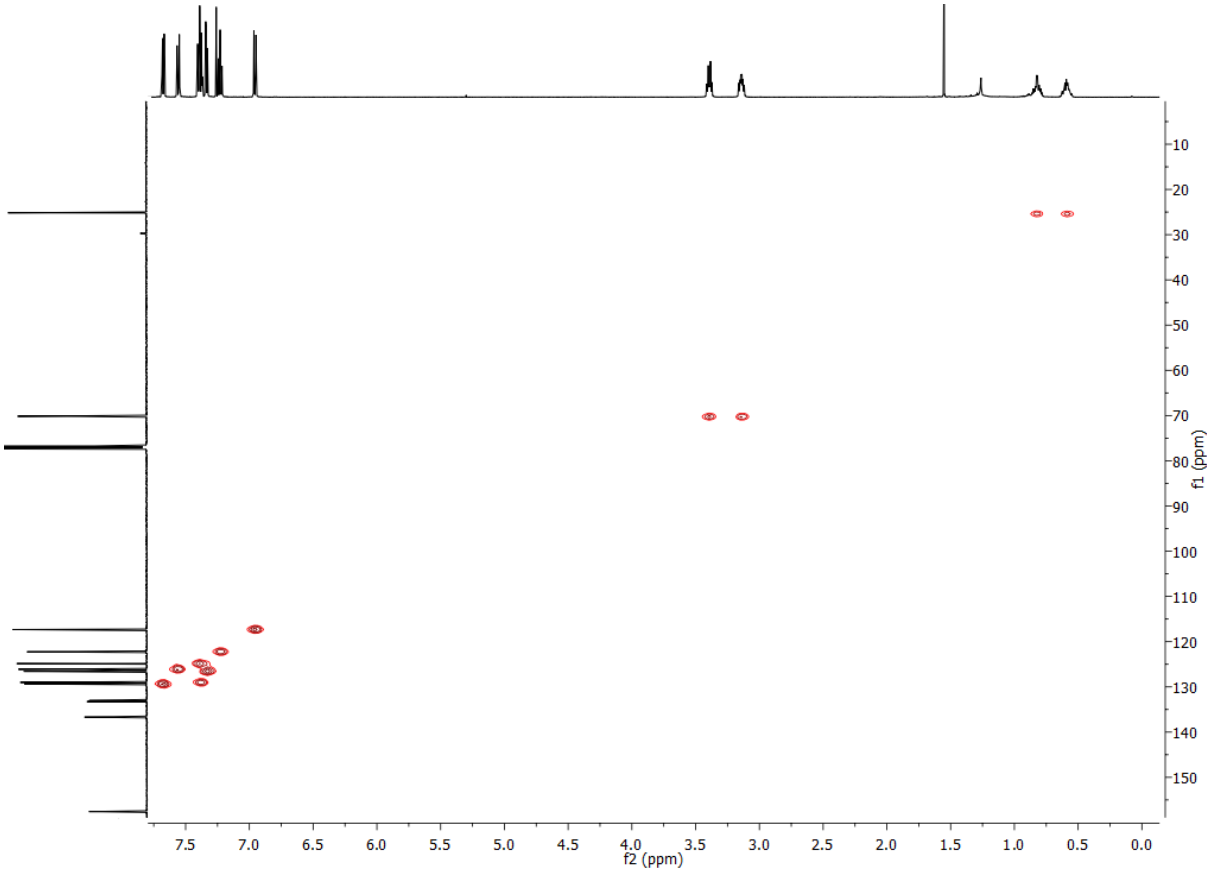

Figure S29. HSQC NMR of **Nap-C4** in $CDCl_3$ at 298 K.

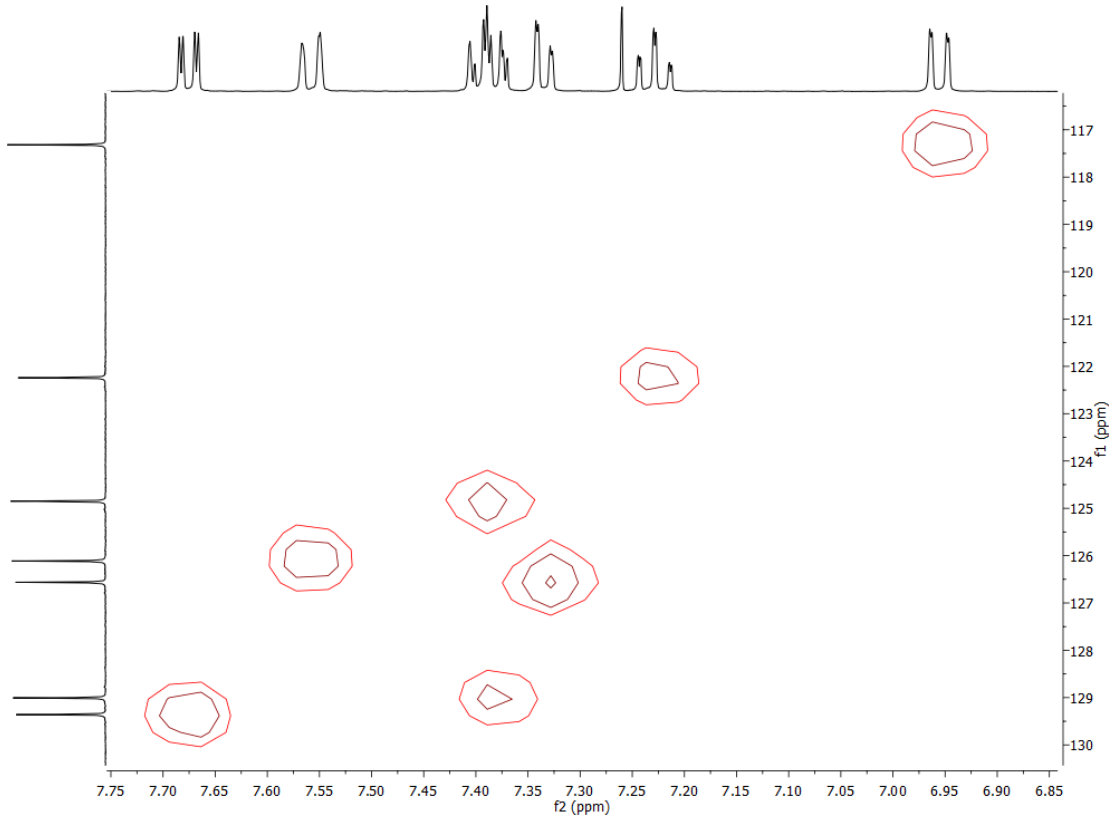

Figure S30. HSQC NMR of **Nap-C4** in $CDCl_3$ at 298 K. Expansion of the aromatic region.

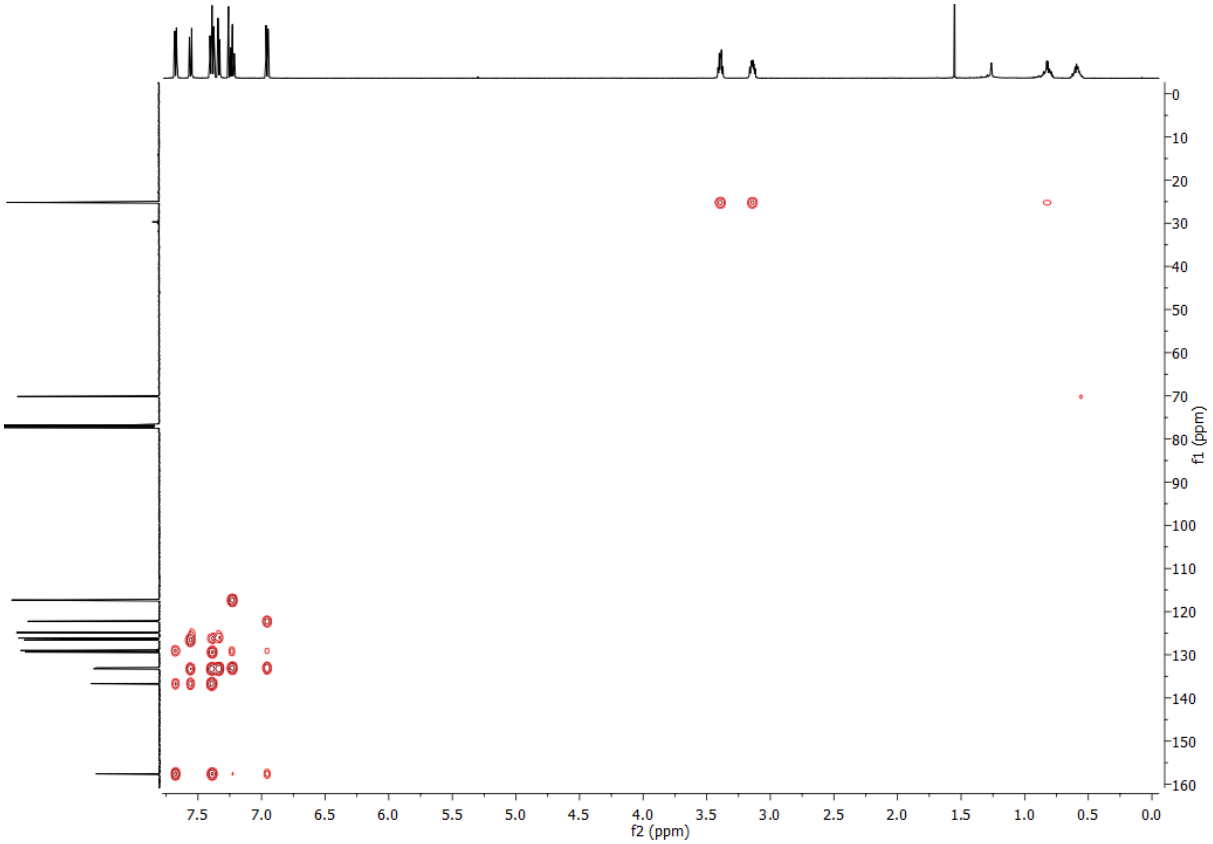

Figure S31. HMBC NMR of **Nap-C4** in $CDCl_3$ at 298 K.

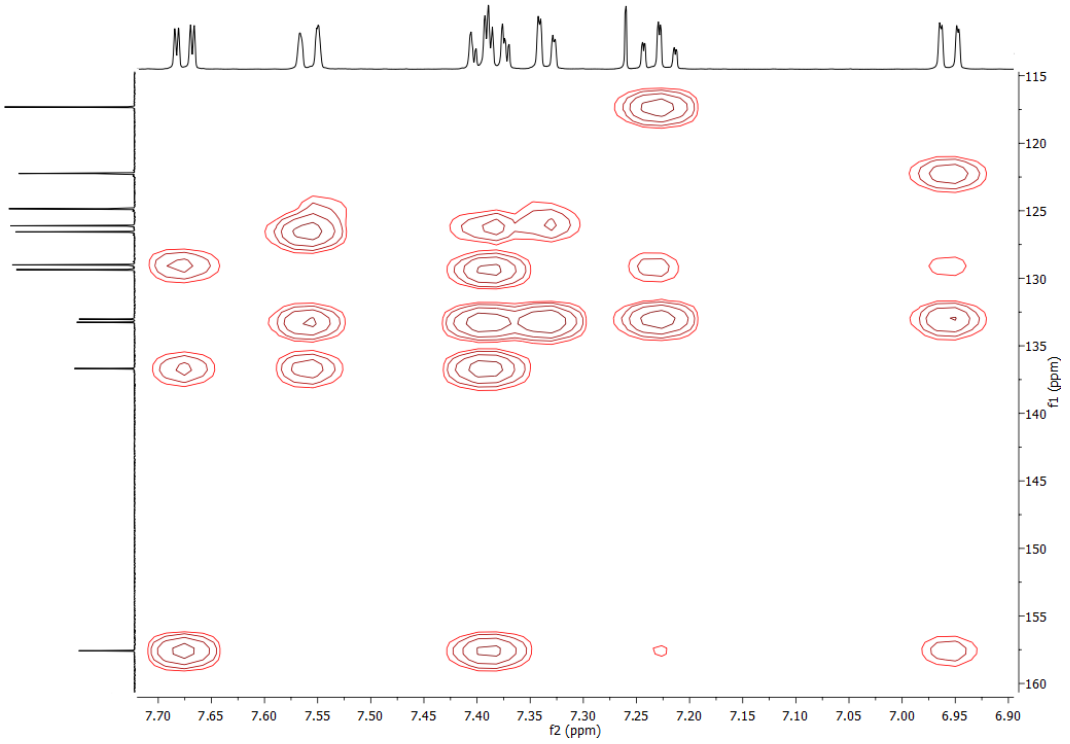

Figure S32. HMBC NMR of **Nap-C4** in $CDCl_3$ at 298 K. Expansion of the aromatic region.

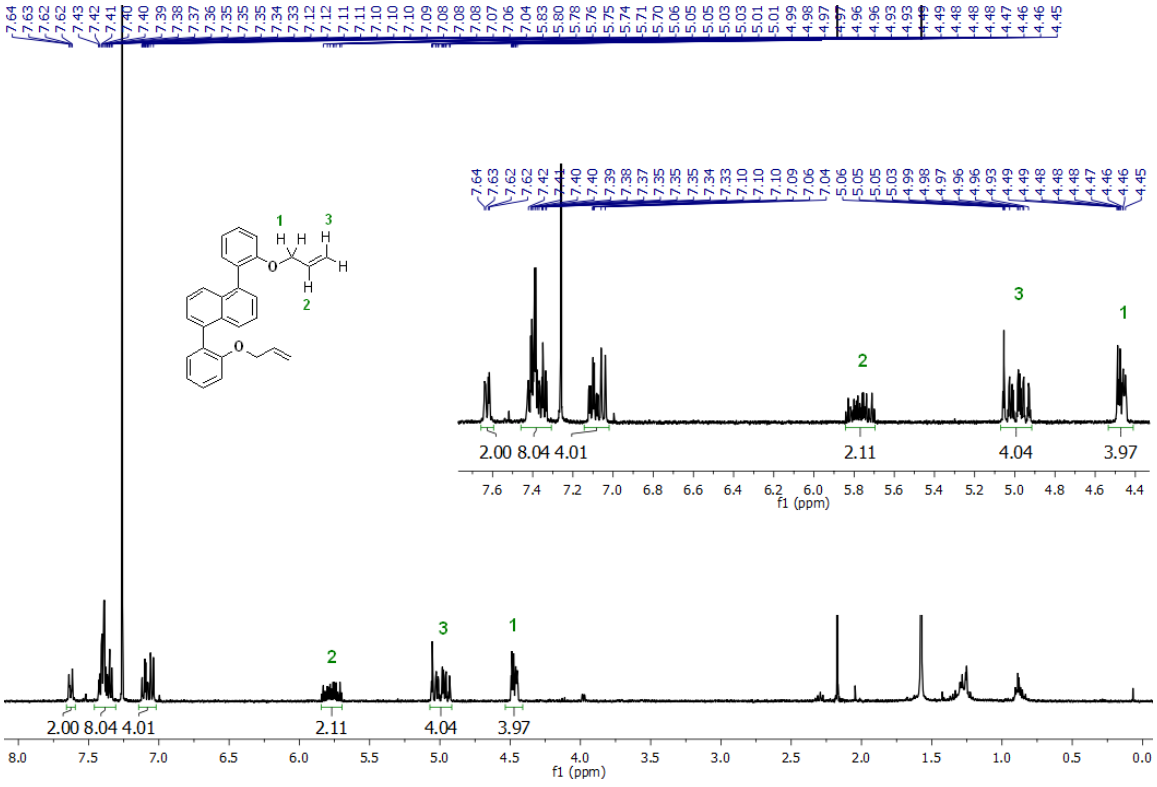

Figure S33. ^1H NMR of compound **5** in $CDCl_3$ at 298 K.

S1.5 Characterization of compound 7

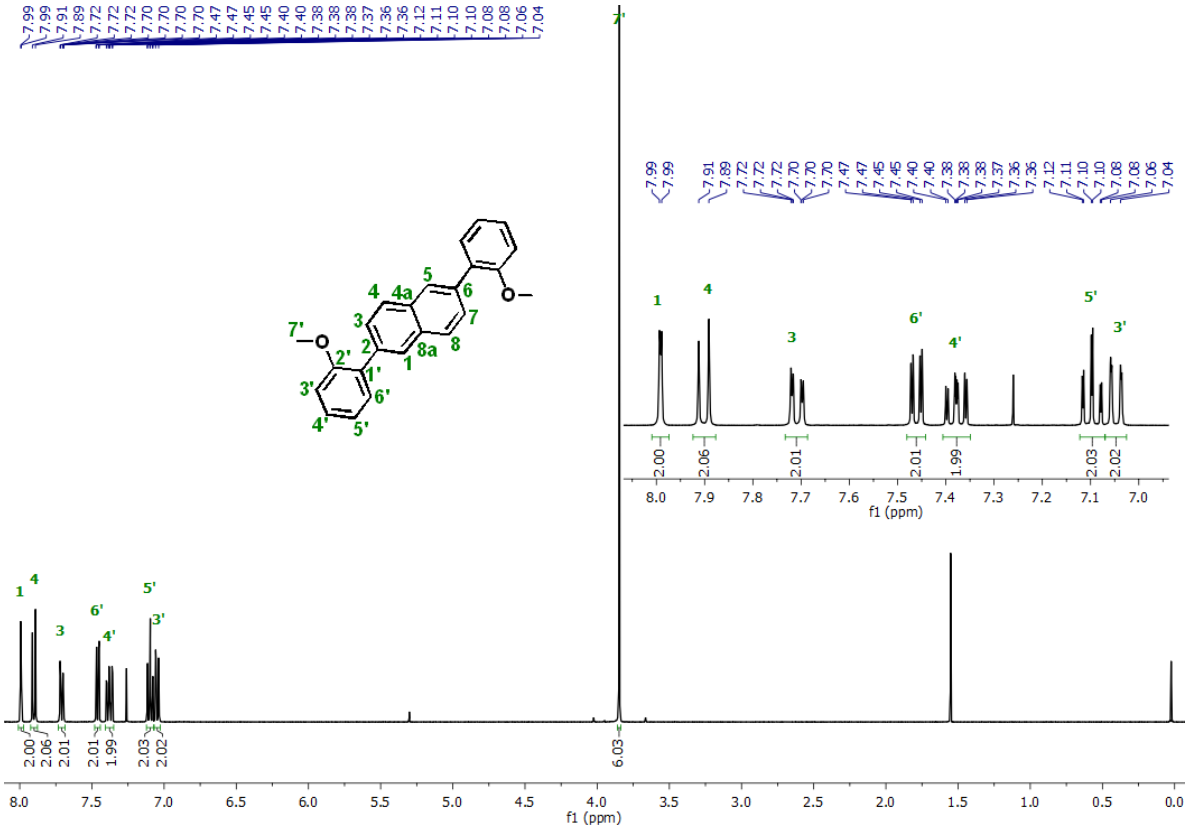

Figure S34. ^{1}H NMR of compound **7** in $CDCl_3$ at 298 K.

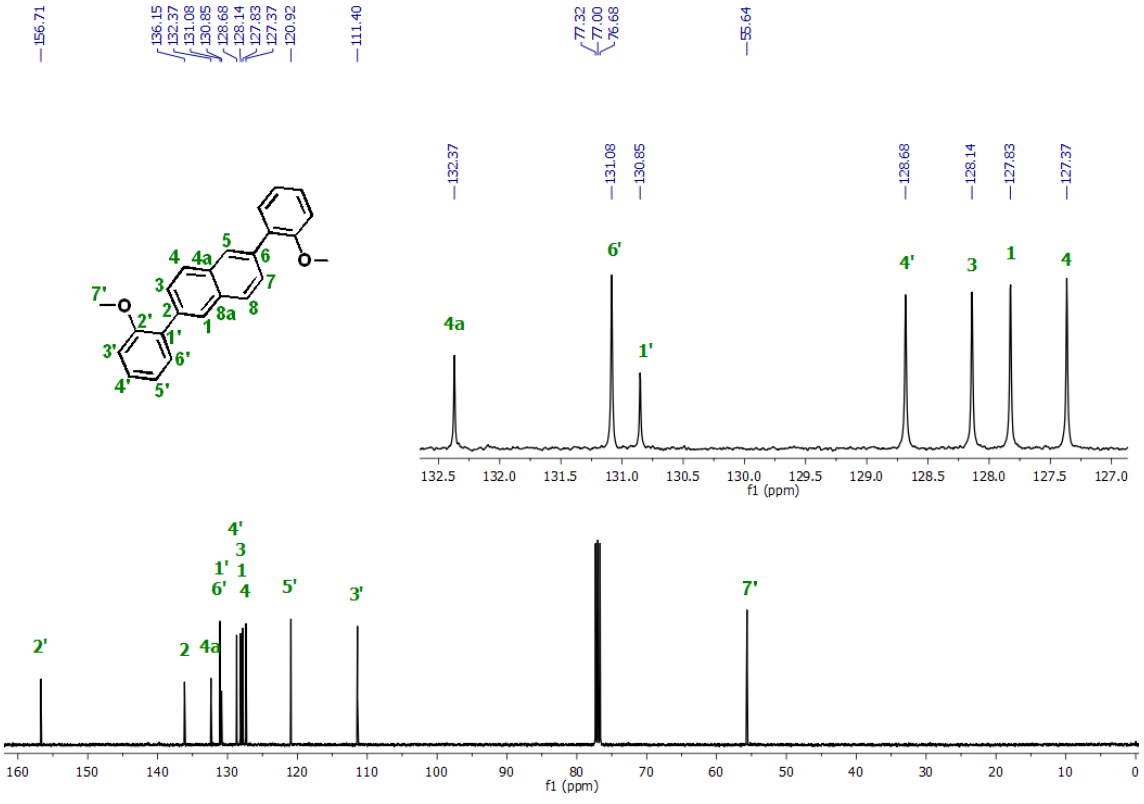

Figure S35. ^{13}C NMR of compound **7** in $CDCl_3$ at 298 K.

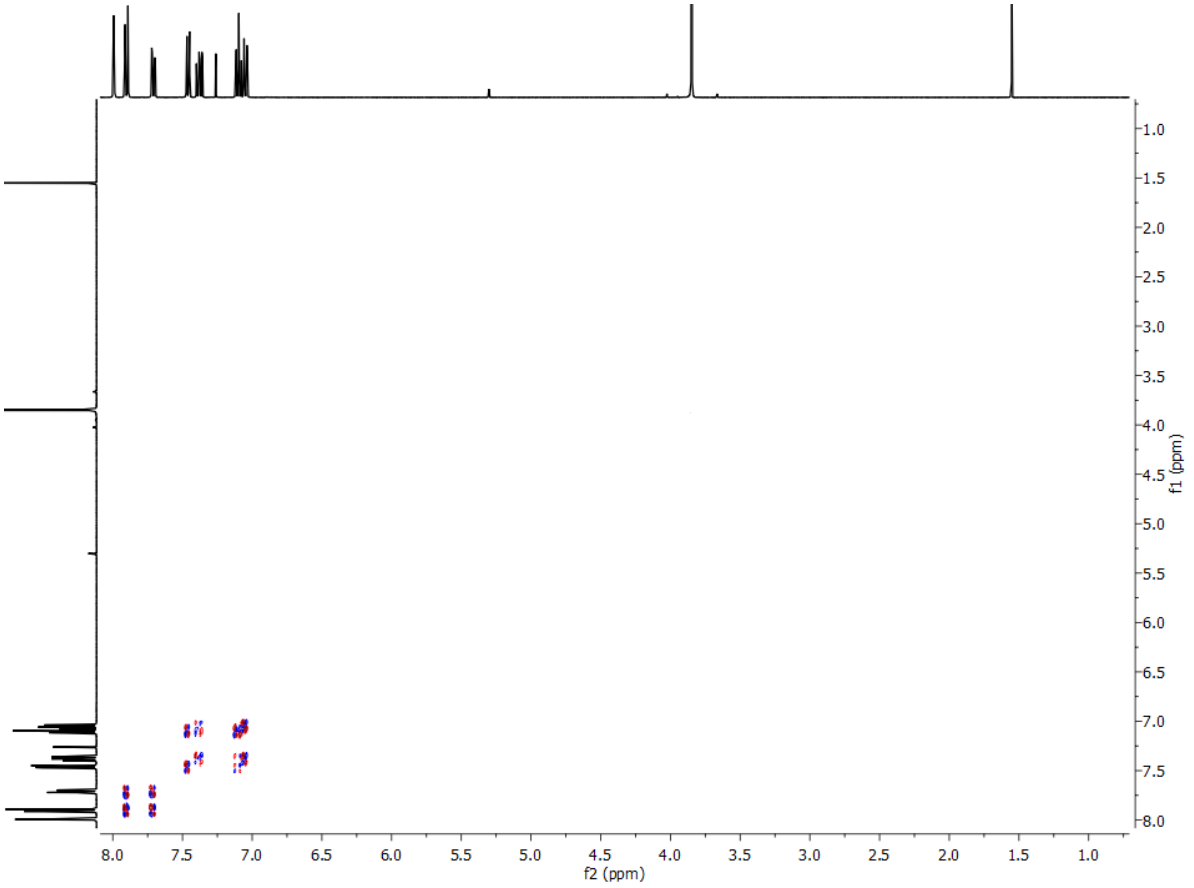

Figure S36. COSY NMR of compound **5** in $CDCl_3$ at 298 K.

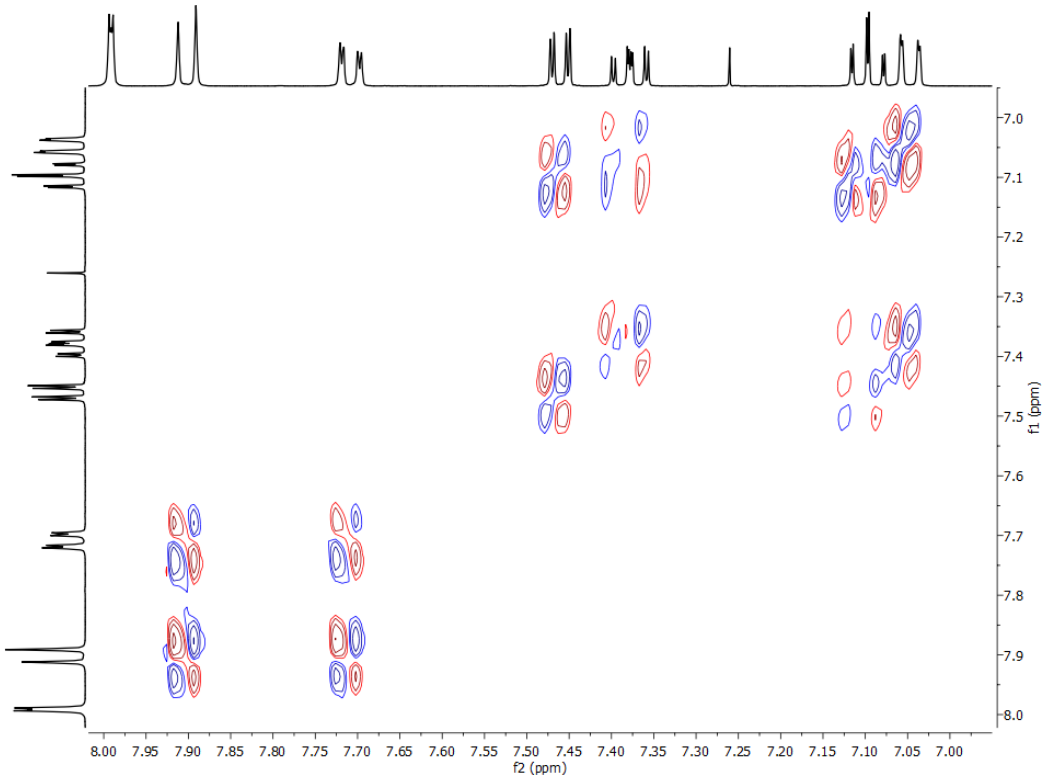

Figure S37. COSY NMR of compound **7** in $CDCl_3$ at 298 K. Expansion of the aromatic region.

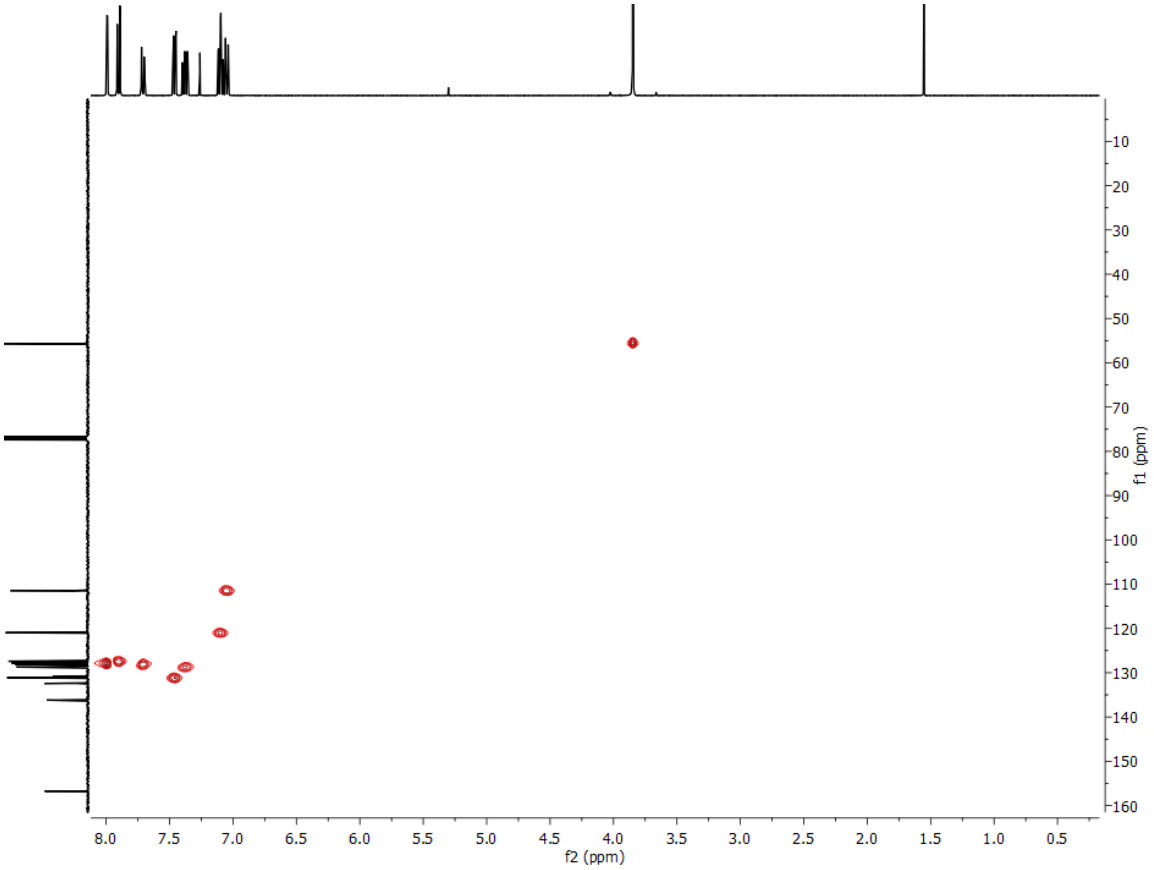

Figure S38. HSQC NMR of compound **7** in $CDCl_3$ at 298 K.

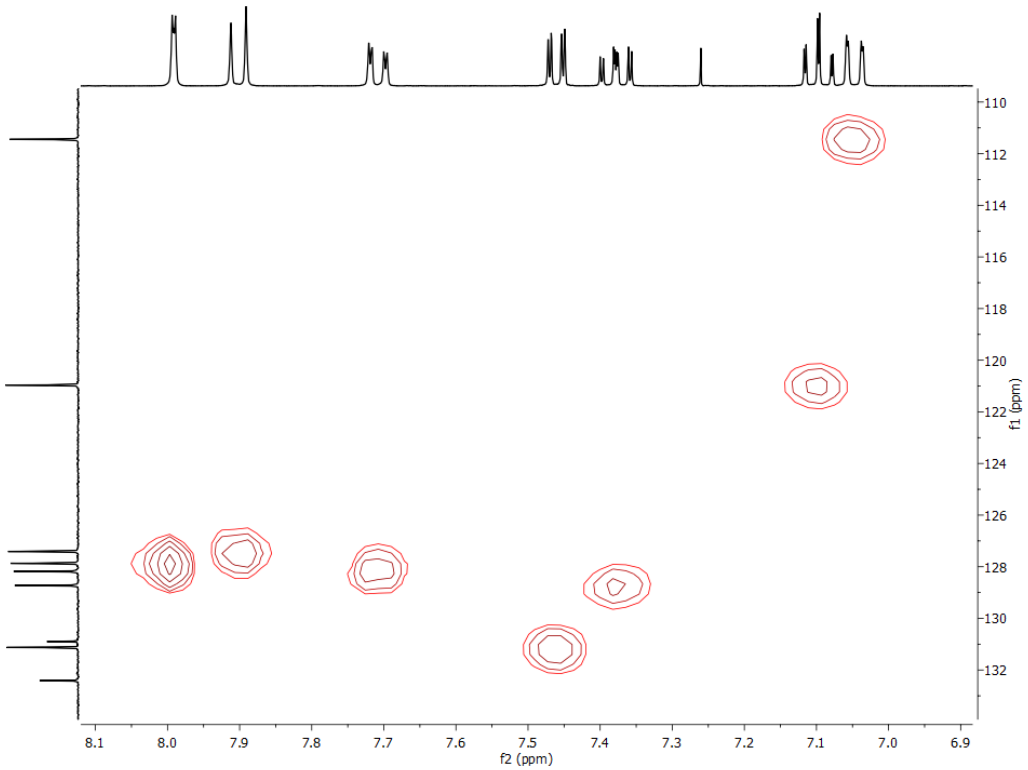

Figure S39. HSQC NMR of compound **7** in $CDCl_3$ at 298 K. Expansion of the aromatic region.

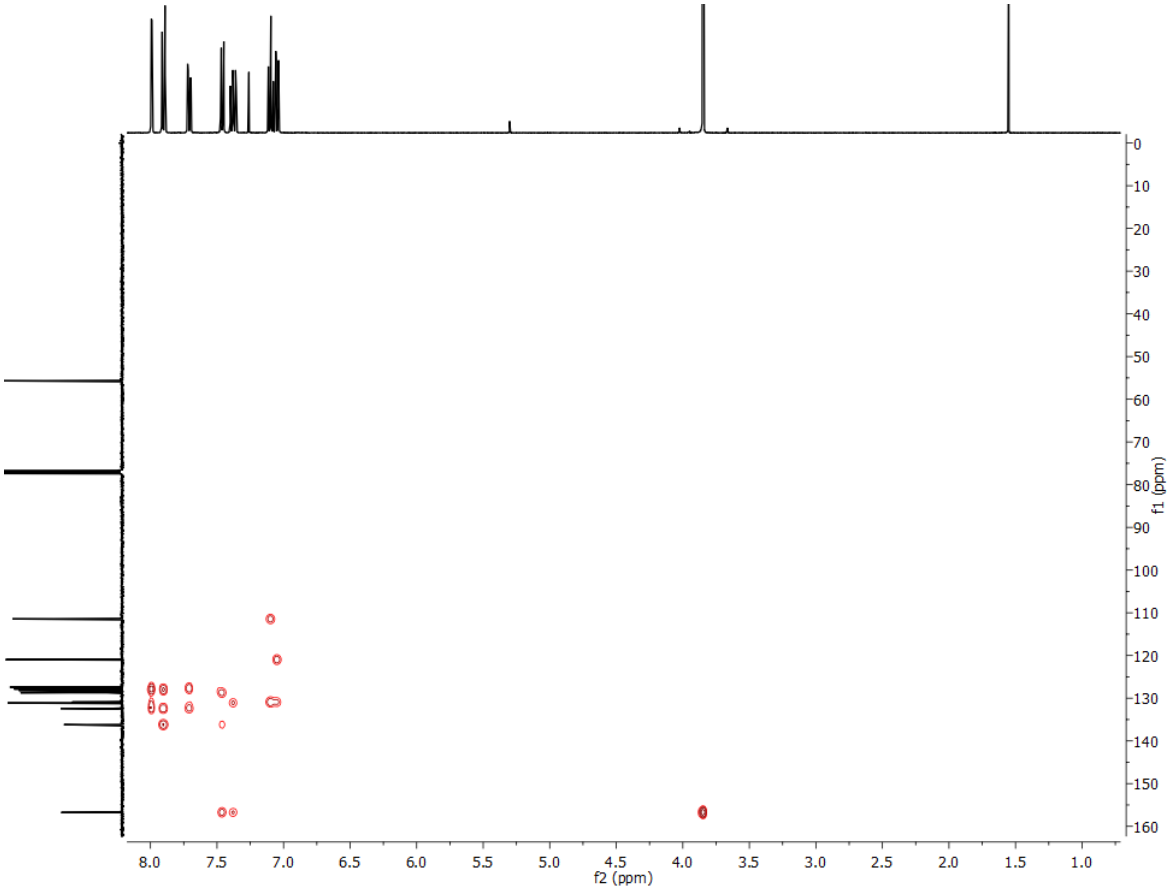

Figure S40. HMBC NMR of compound **7** in $CDCl_3$ at 298 K.

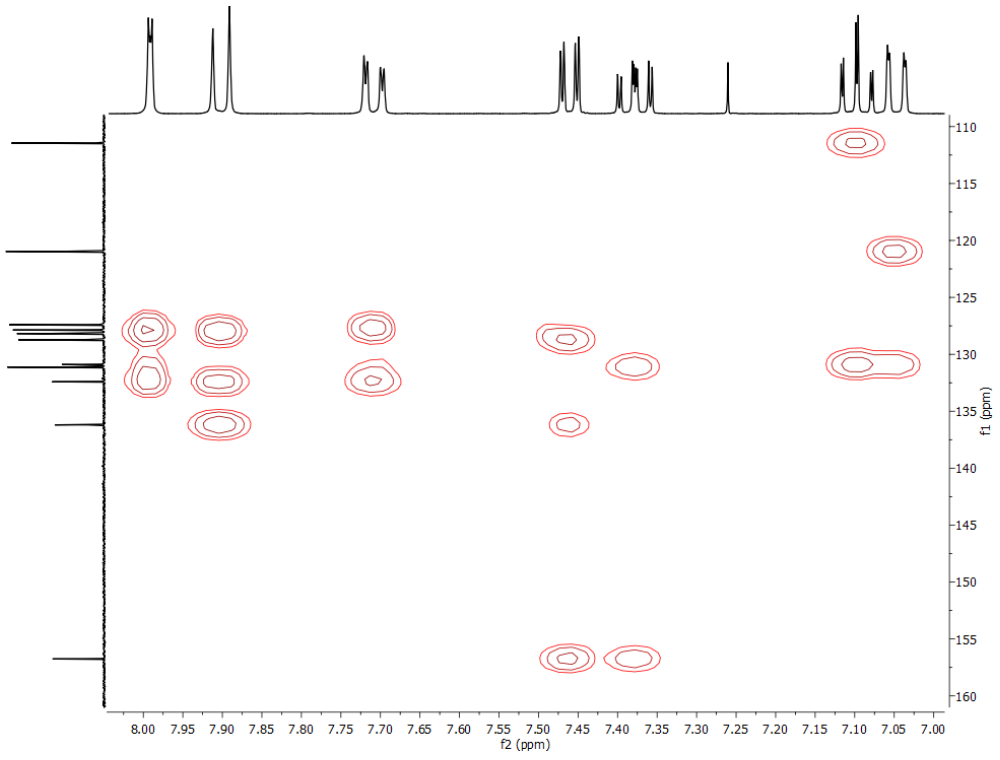

Figure S41. HMBC NMR of compound **7** in $CDCl_3$ at 298 K. Expansion of the aromatic region.

S1.6 Characterization of compound 8

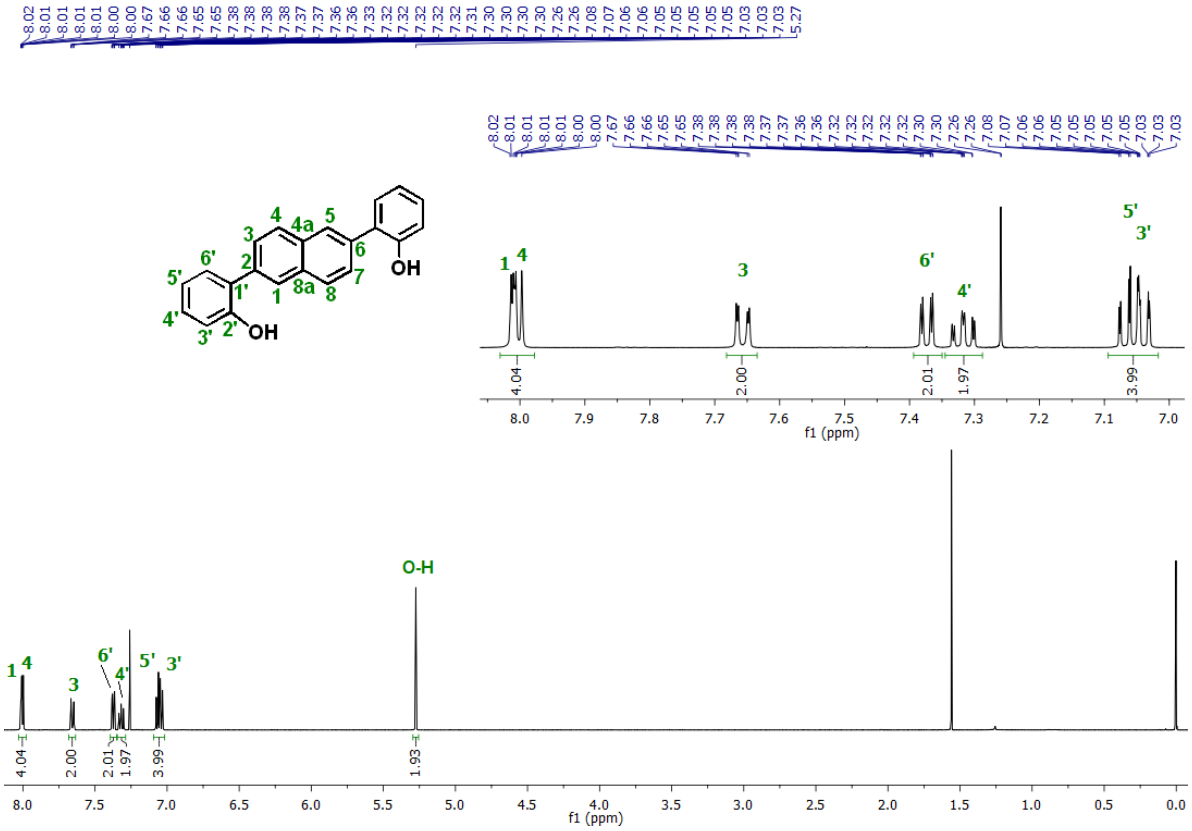

Figure S42. ^{1}H NMR of compound **8** in $CDCl_3$ at 298 K.

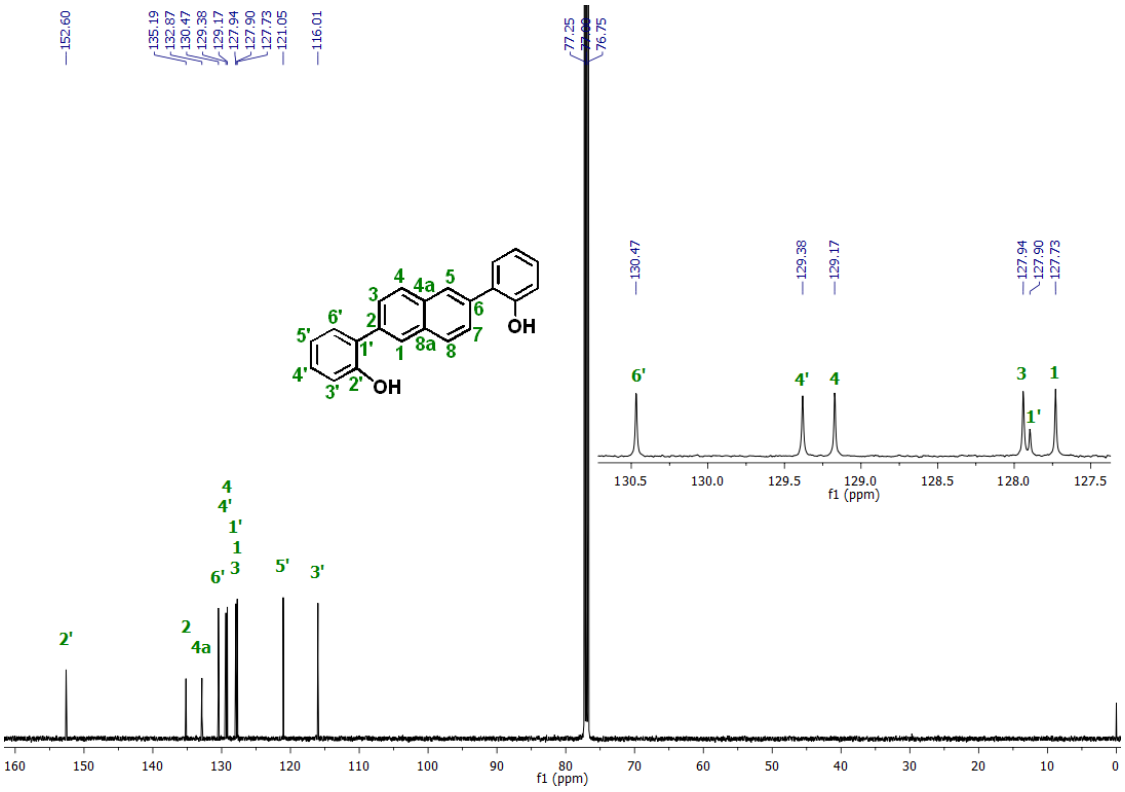

Figure S43. ^{13}C NMR of compound **8** in $CDCl_3$ at 298 K.

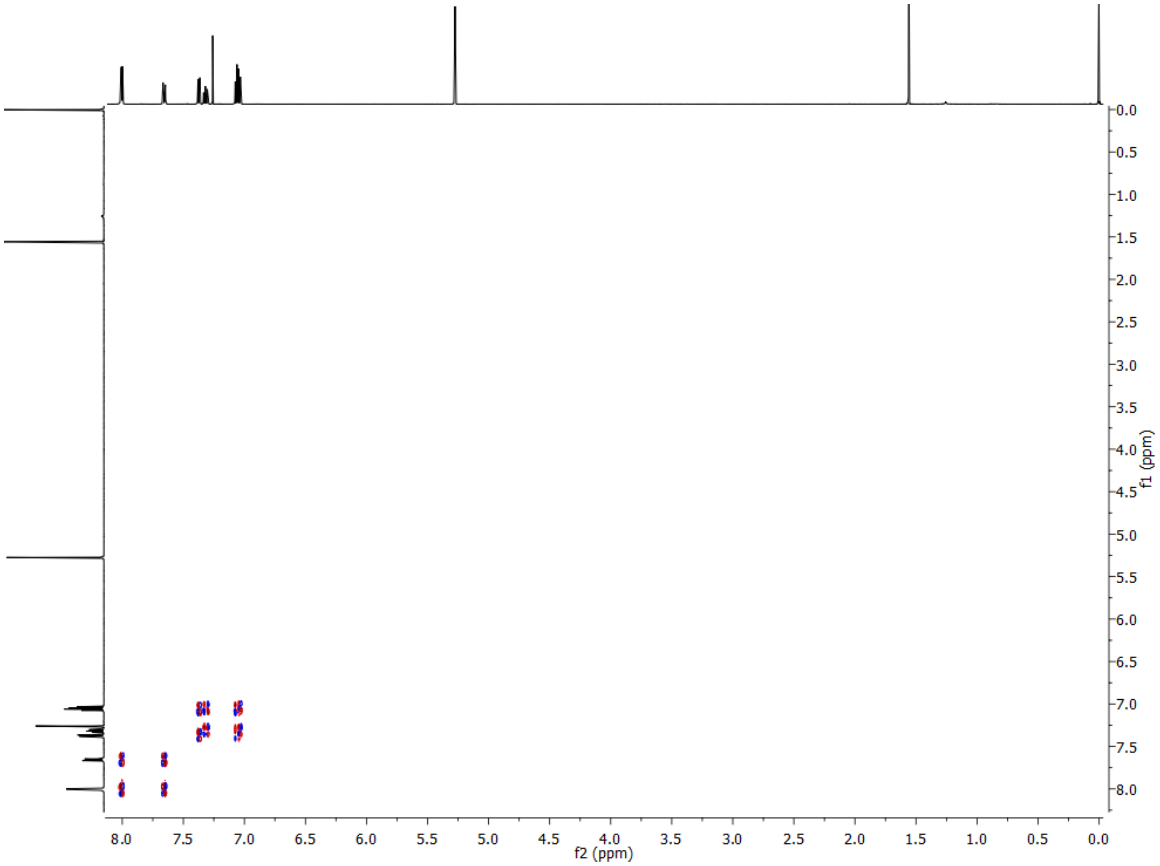

Figure S44. COSY NMR of compound **8** in $CDCl_3$ at 298 K.

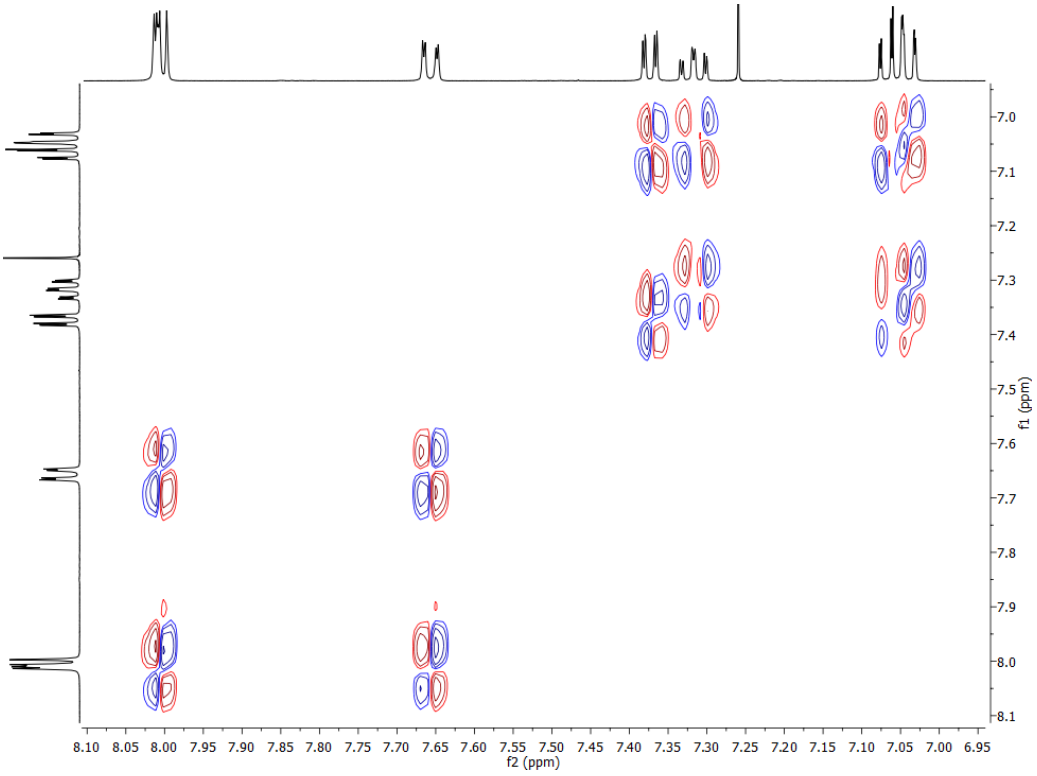

Figure S45. COSY NMR of compound **8** in $CDCl_3$ at 298 K. Expansion of the aromatic region.

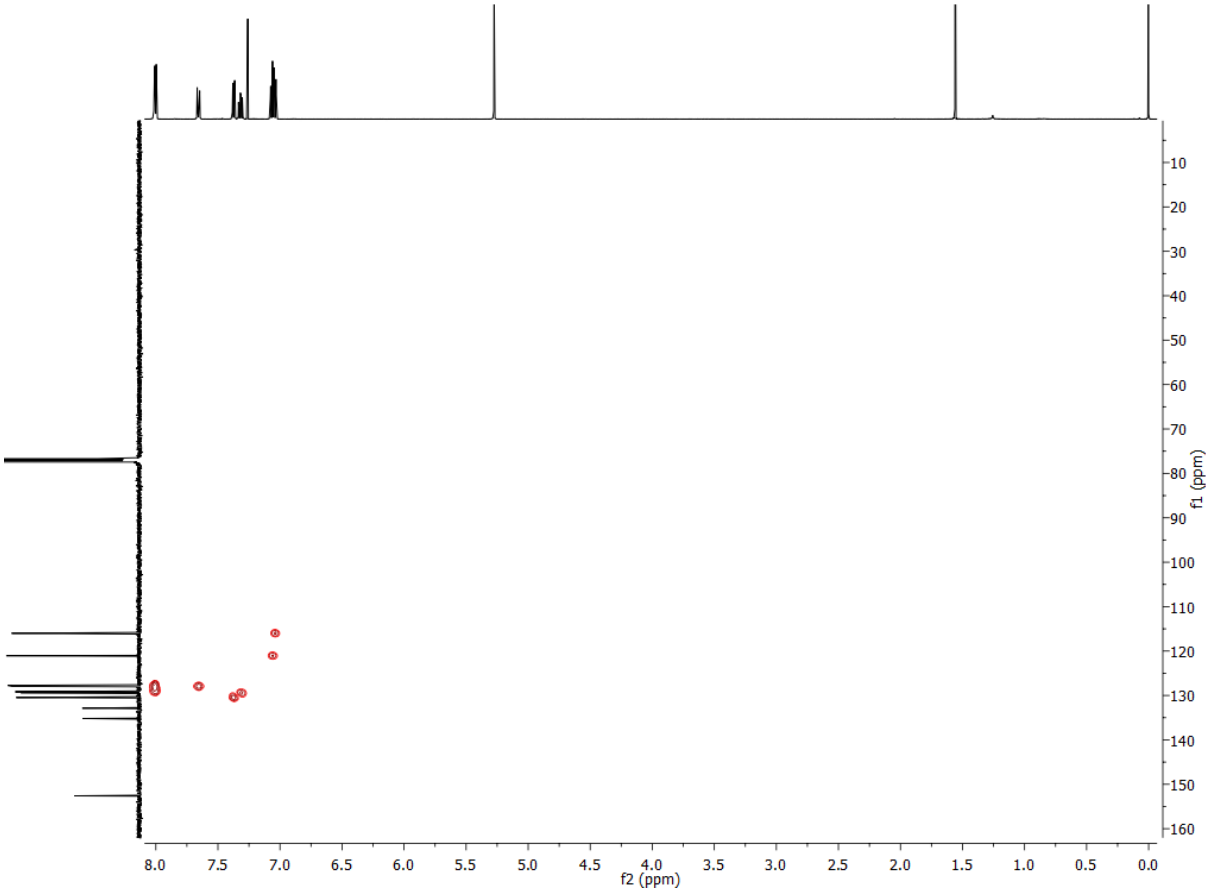

Figure S46. HSQC NMR of compound **8** in $CDCl_3$ at 298 K.

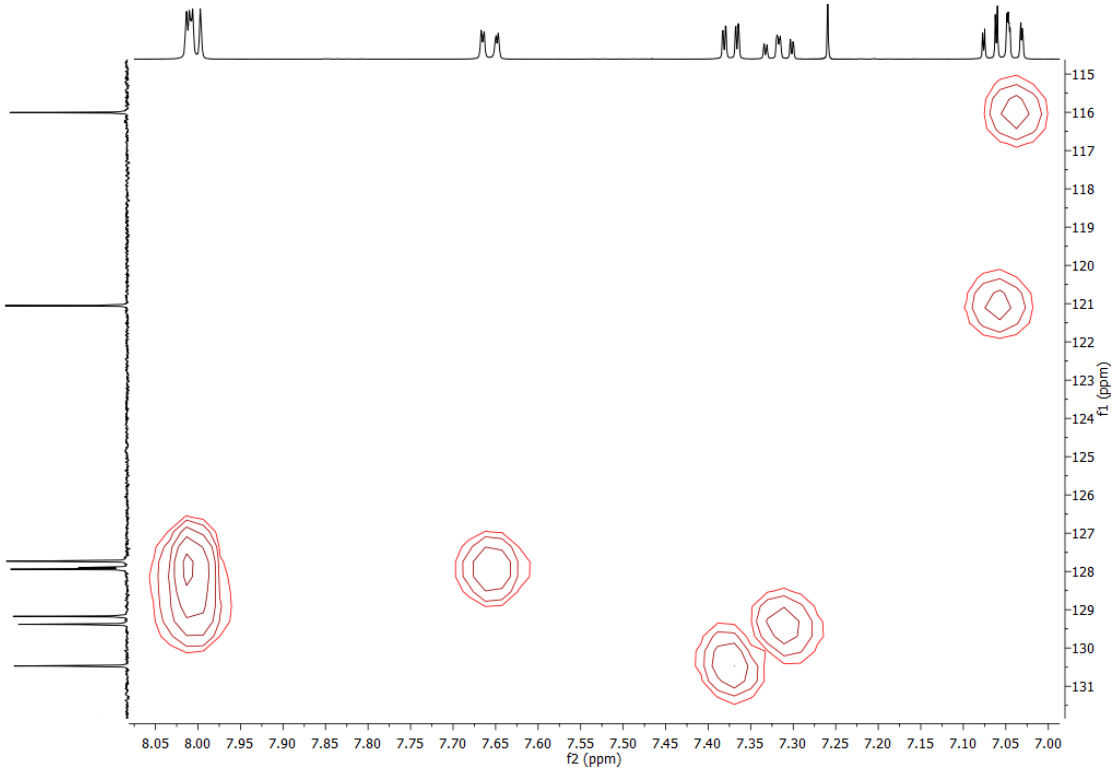

Figure S47. HSQC NMR of compound **8** in $CDCl_3$ at 298 K. Expansion of the aromatic region.

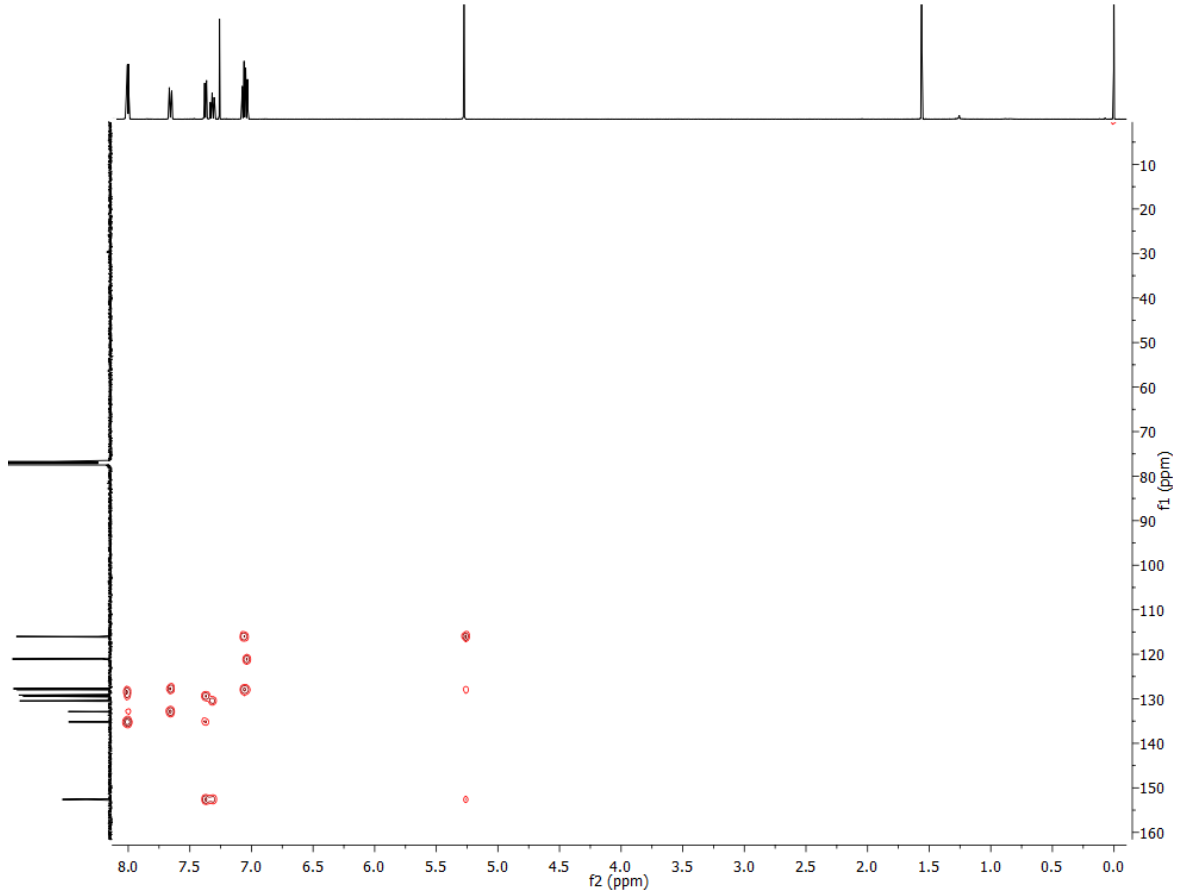

Figure S48. HMBC NMR of compound **8** in $CDCl_3$ at 298 K.

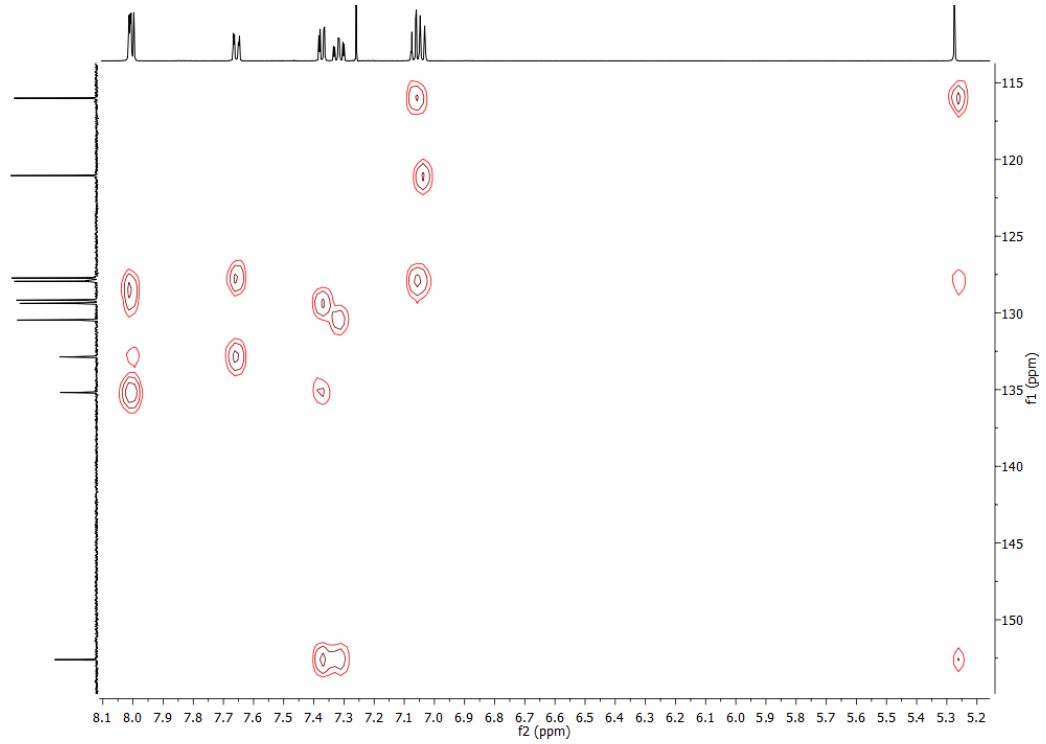

Figure S49. HMBC NMR of compound **8** in $CDCl_3$ at 298 K. Expansion of the aromatic region.

S1.6 Characterization of Cyc-C6

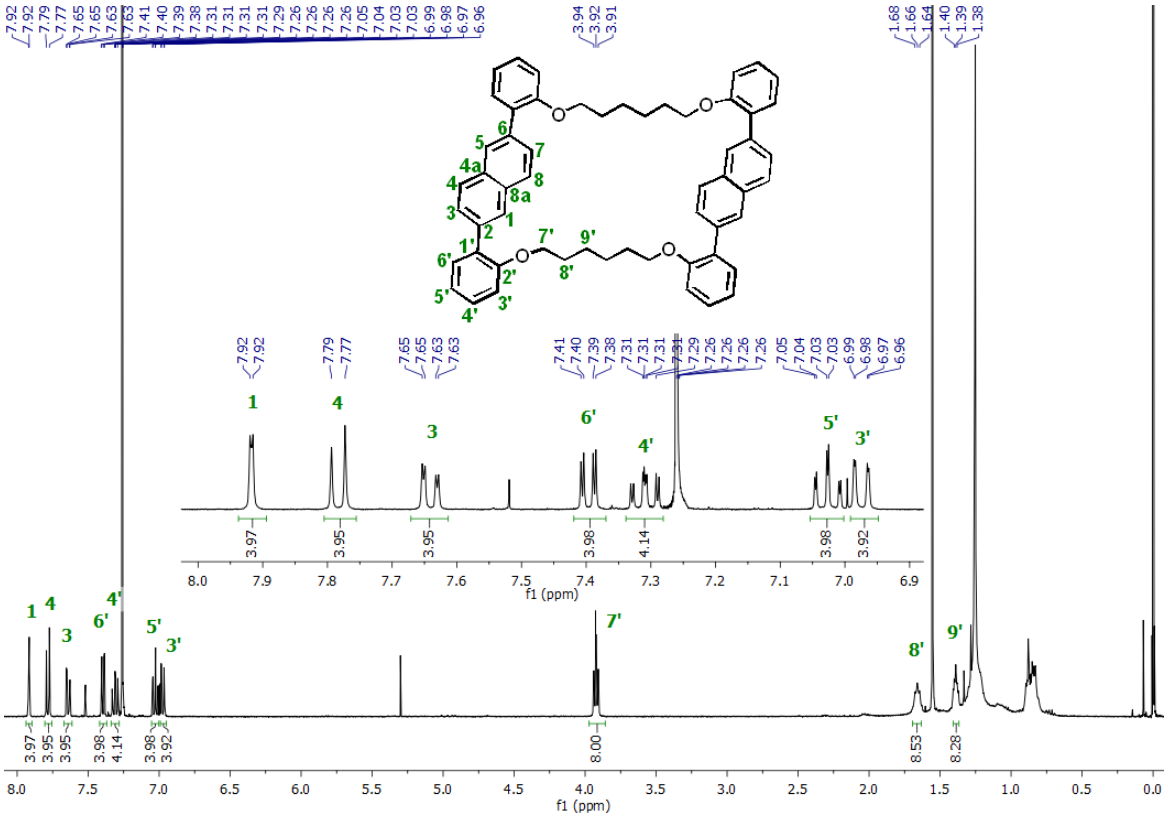

Figure S50. ^{1}H NMR of **Cyc-C6** in $CDCl_3$ at 298 K.

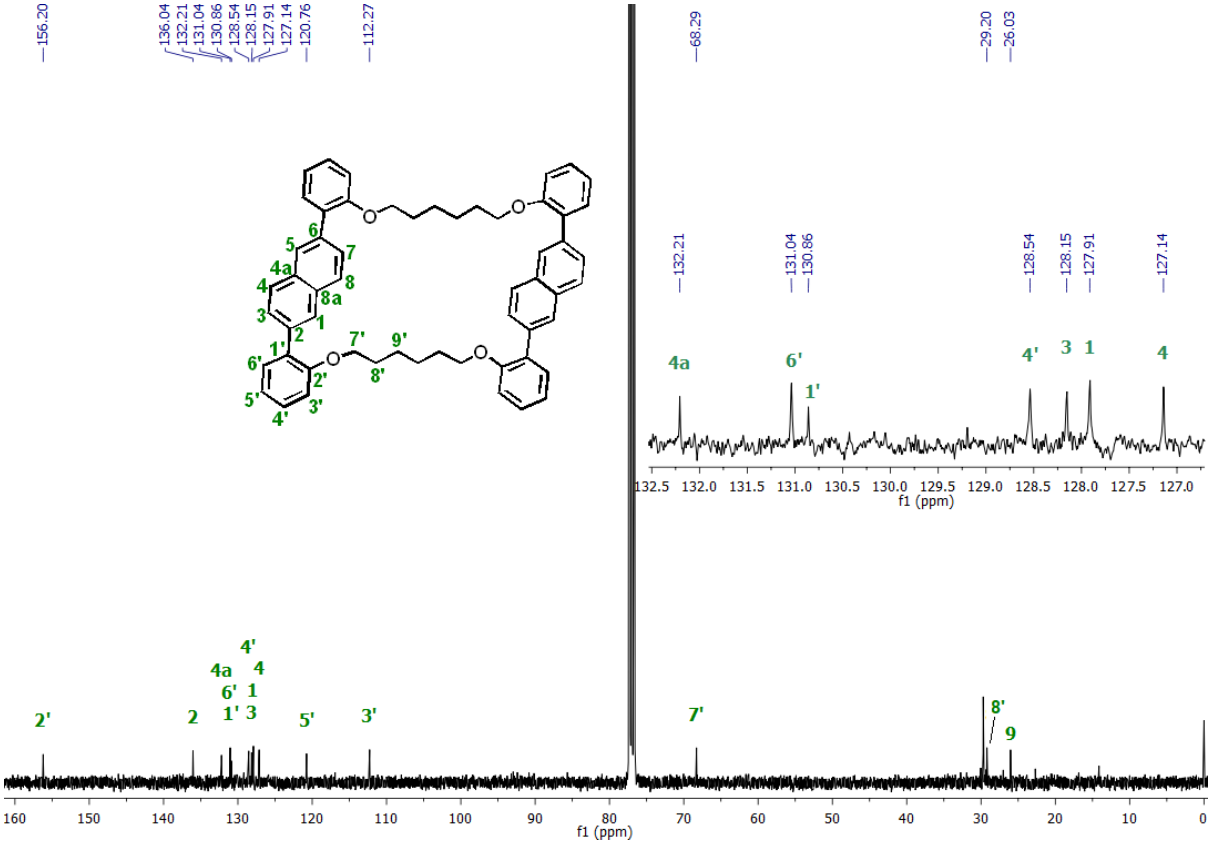

Figure S51. ^{13}C NMR of **Cyc-C6** in $CDCl_3$ at 298 K.

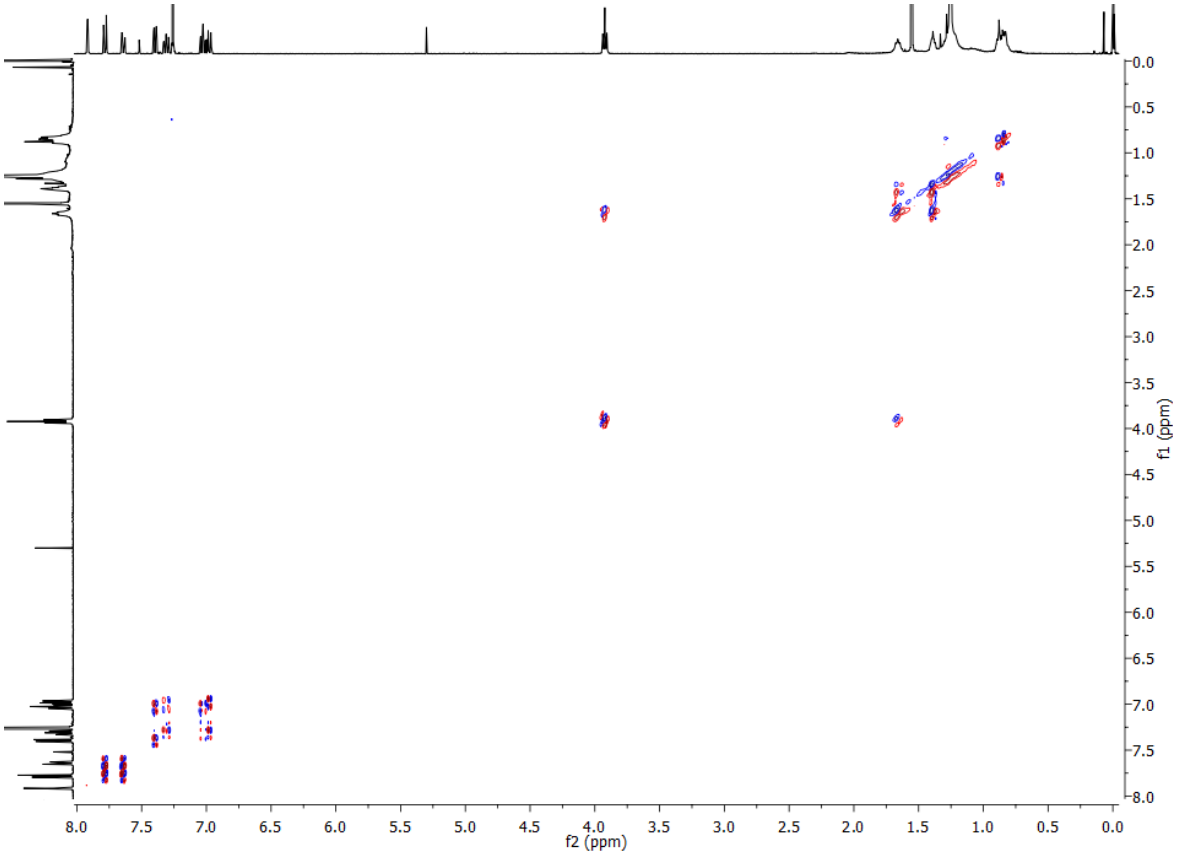

Figure S52. COSY NMR of **Cyc-C6** in $CDCl_3$ at 298 K.

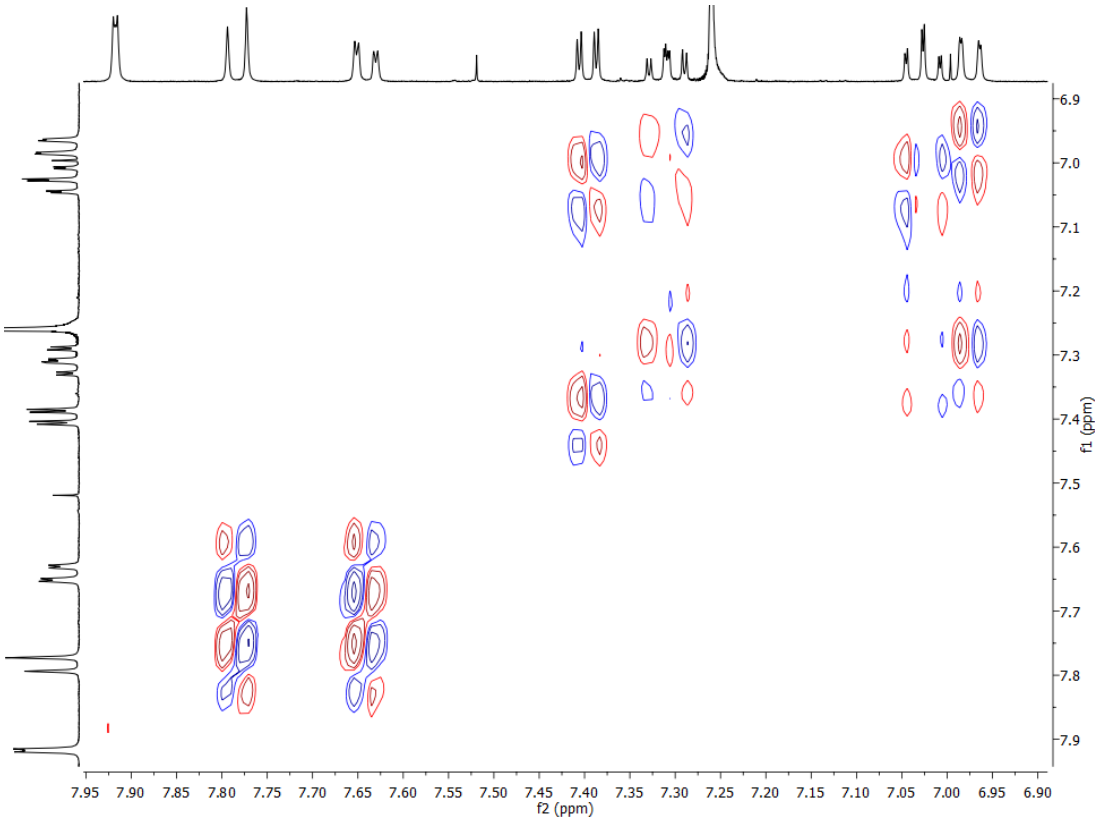

Figure S53. COSY NMR of **Cyc-C6** in $CDCl_3$ at 298 K. Expansion of the aromatic region.

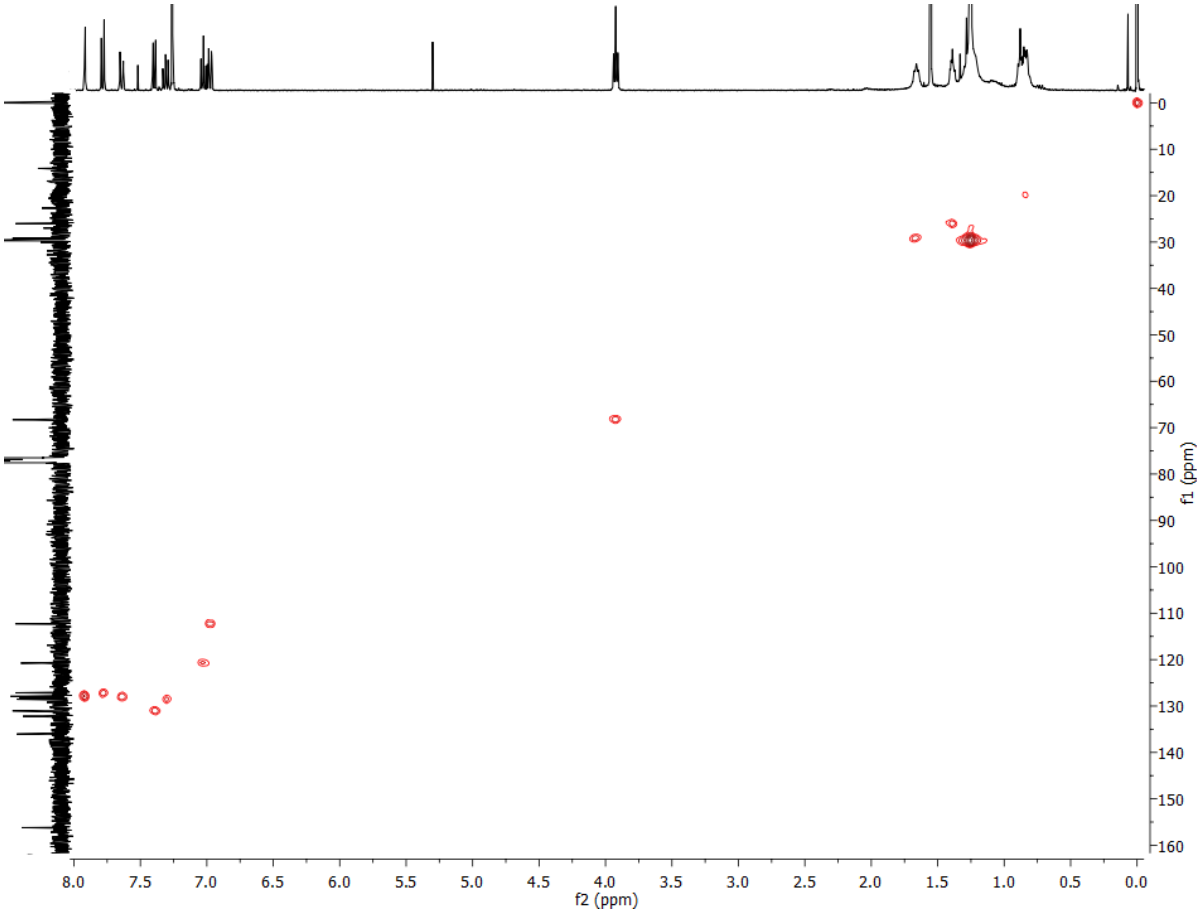

Figure S54. HSQC NMR of **Cyc-C6** in $CDCl_3$ at 298 K.

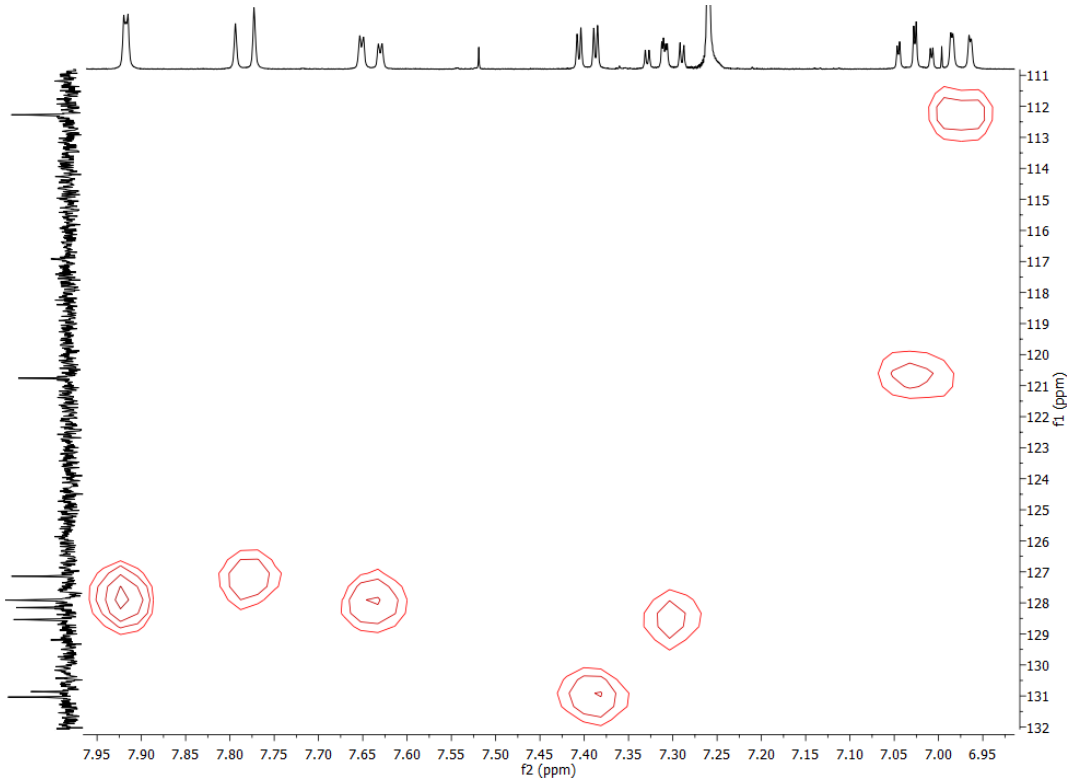

Figure S55. HSQC NMR of **Cyc-C6** in $CDCl_3$ at 298 K. Expansion of the aromatic region.

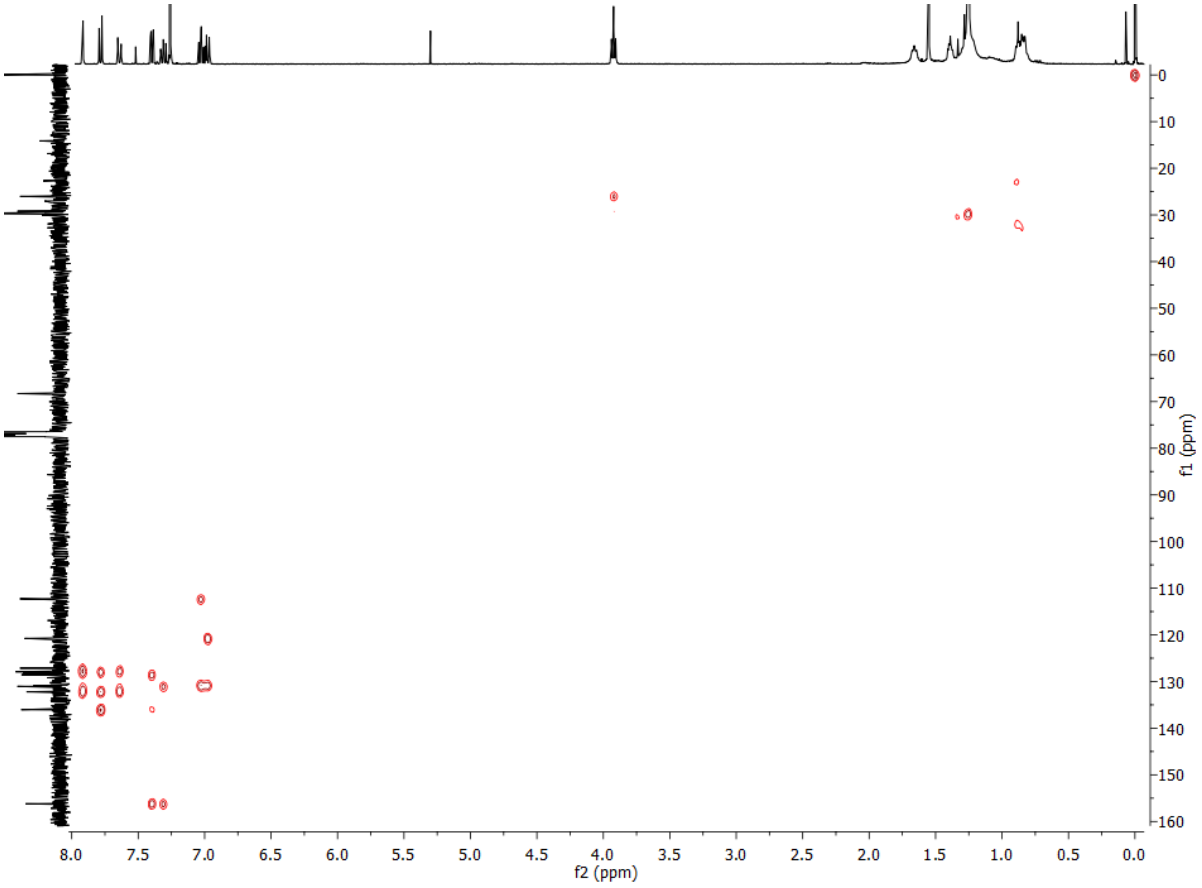

Figure S56. HMBC NMR of **Cyc-C6** in $CDCl_3$ at 298 K.

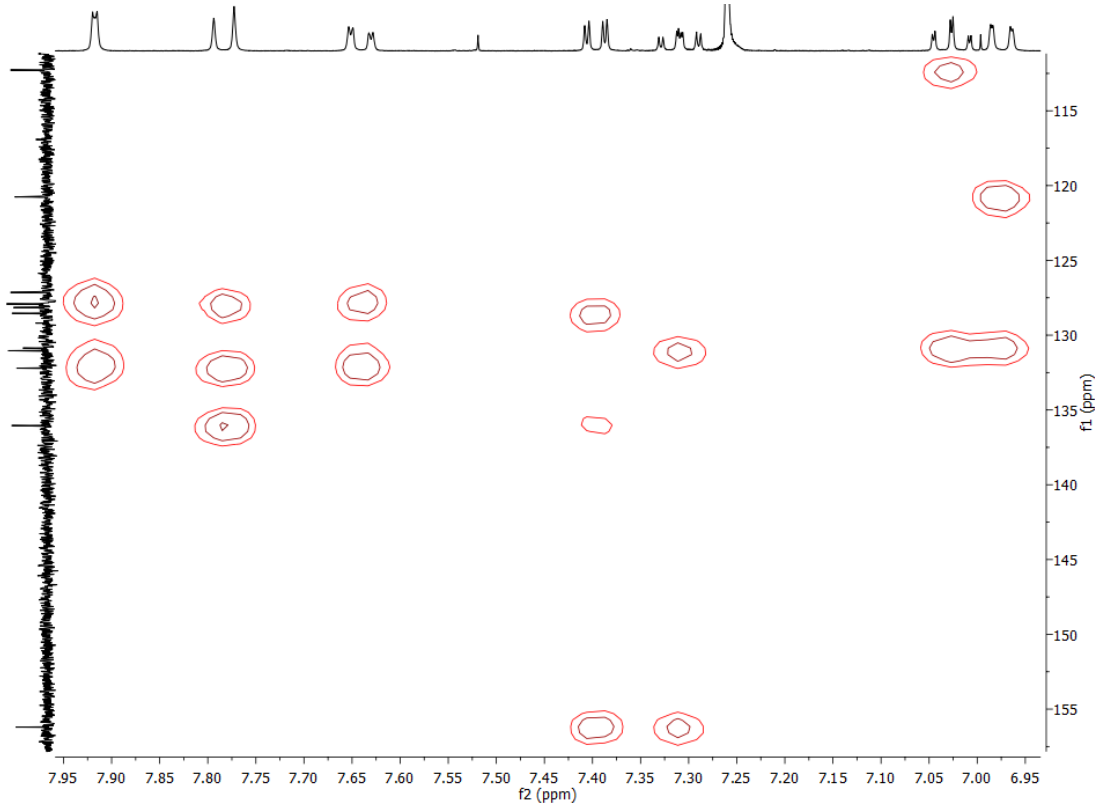

Figure S57. HMBC NMR of **Cyc-C6** in $CDCl_3$ at 298 K. Expansion of the aromatic region.

S1.7 Characterization of Cyc-C4

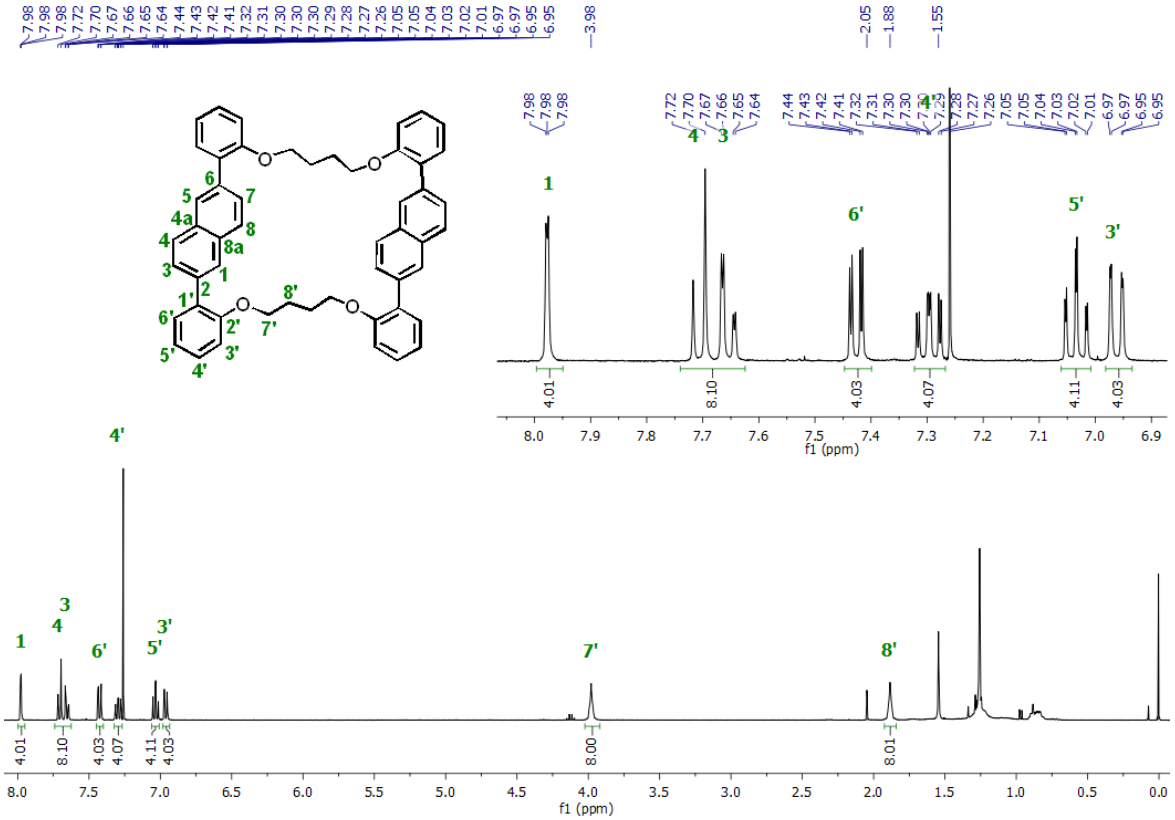

Figure S58: ^{1}H NMR of **Cyc-C6** in $CDCl_3$ at 298 K.

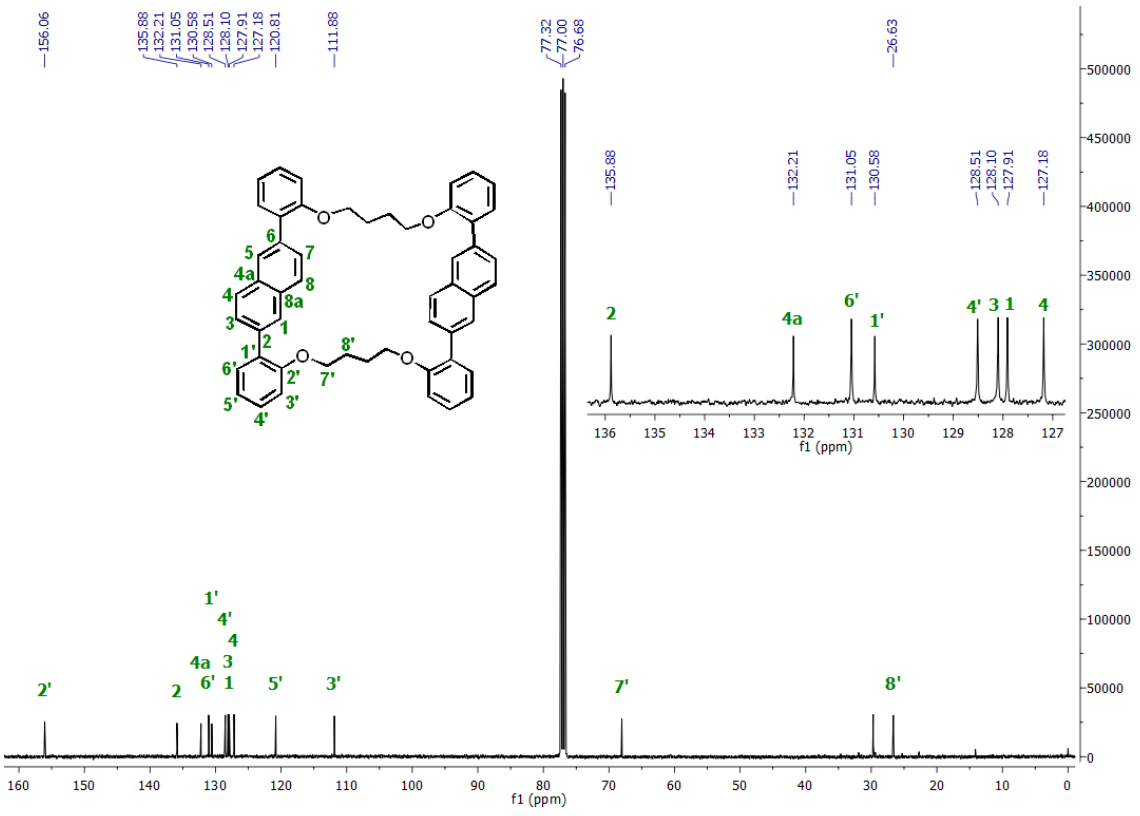

Figure S59. ^{13} CNMR of **Cyc-C4** in $CDCl_3$ at 298 K.

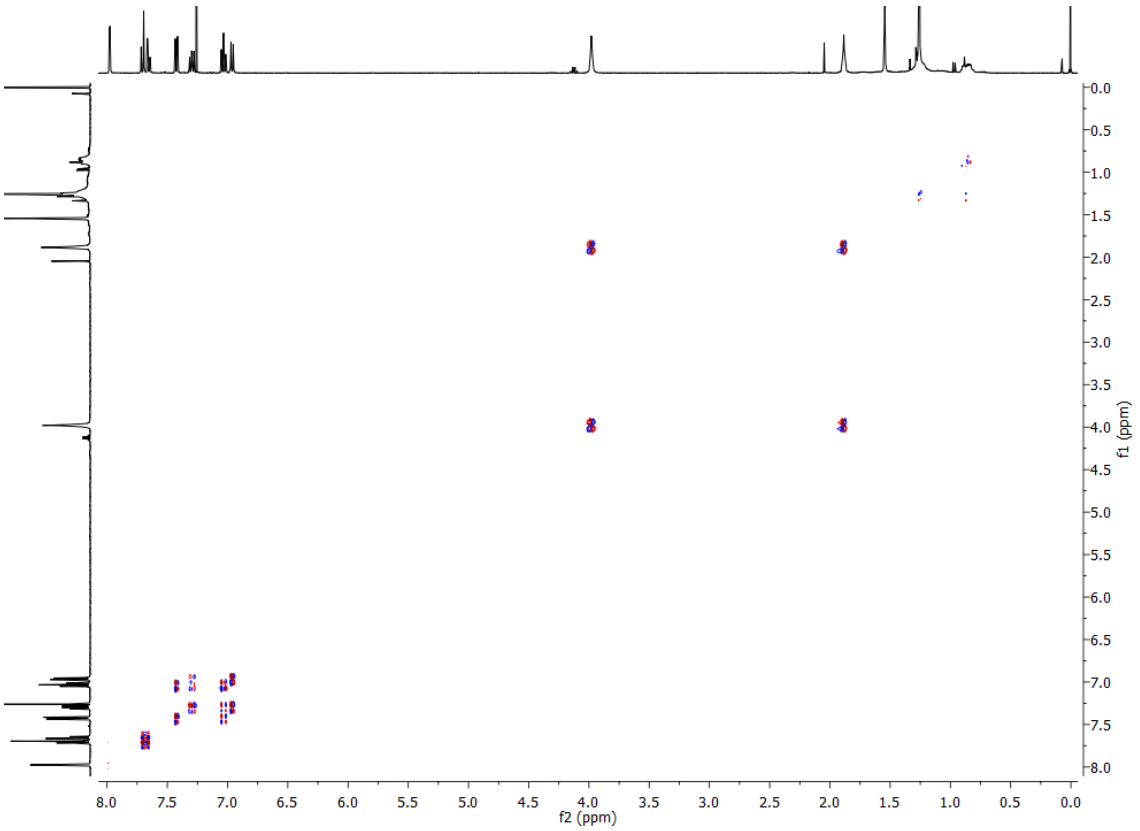

Figure S60. COSY NMR of **Cyc-C4** in $CDCl_3$ at 298 K.

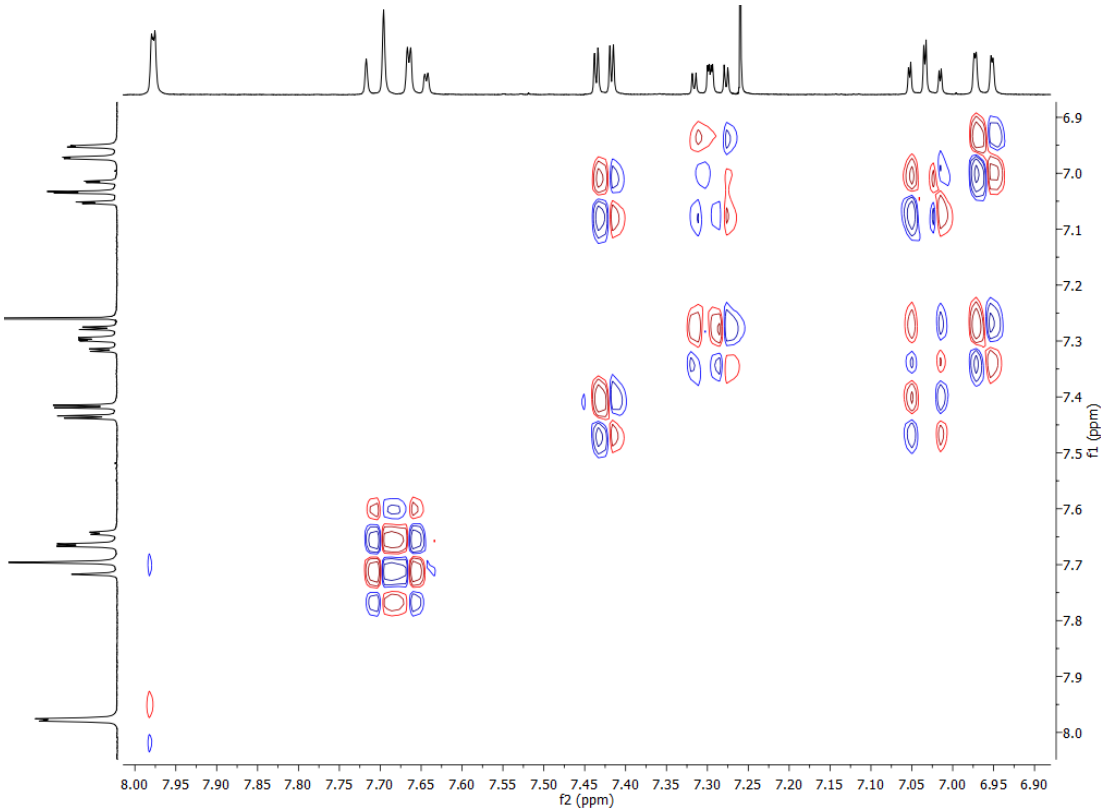

Figure S61. COSY NMR of **Cyc-C4** in $CDCl_3$ at 298 K. Expansion of the aromatic region.

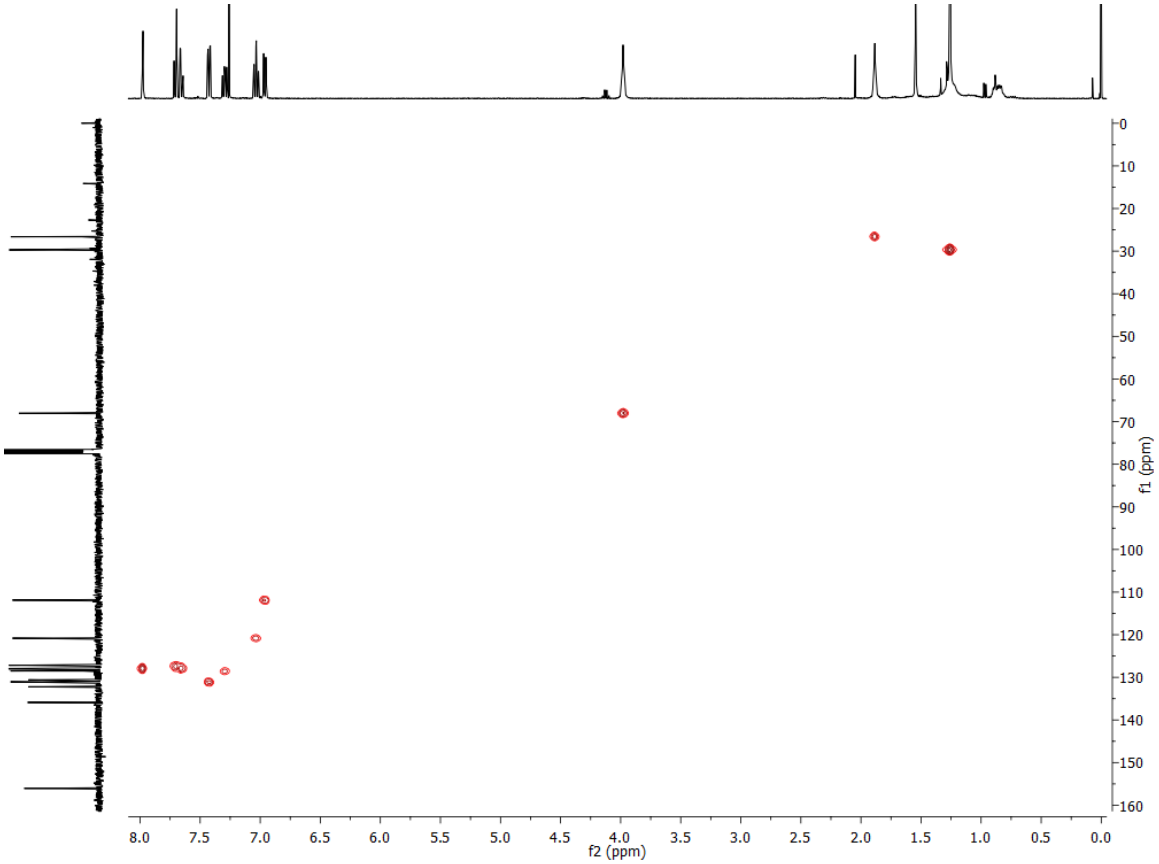

Figure S62. HSQC NMR of **Cyc-C4** in $CDCl_3$ at 298 K.

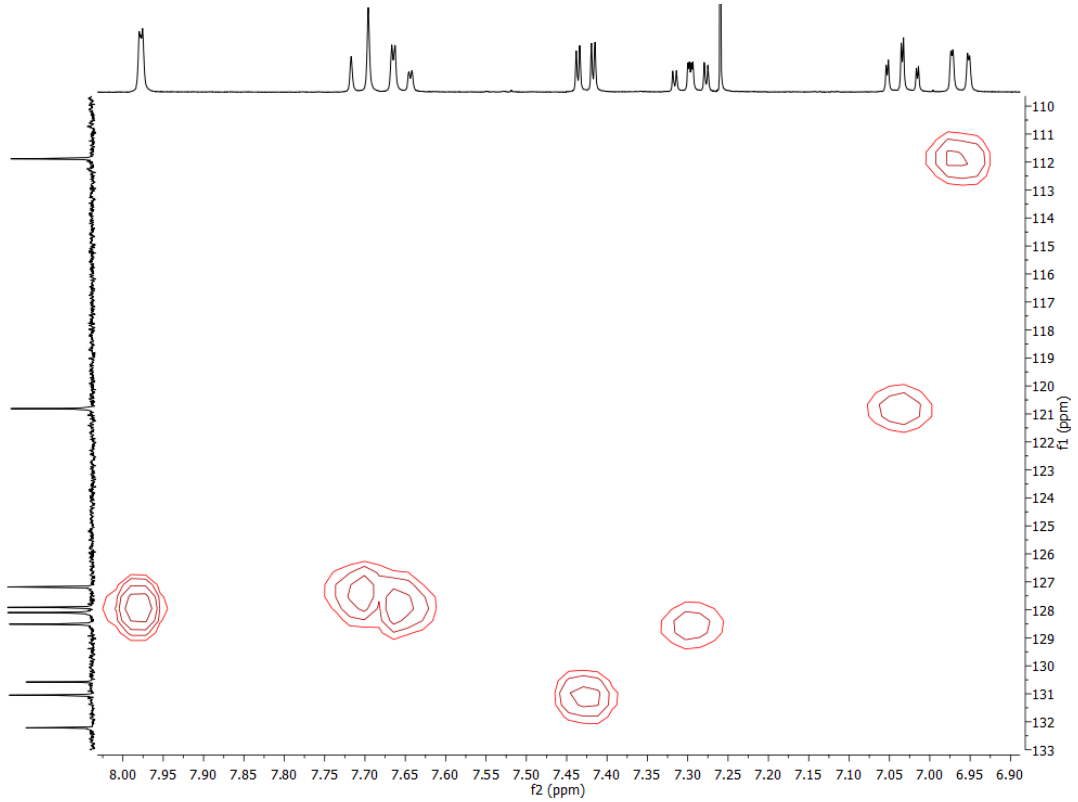

Figure S63. HSQC NMR of **Cyc-C4** in $CDCl_3$ at 298 K. Expansion of the aromatic region.

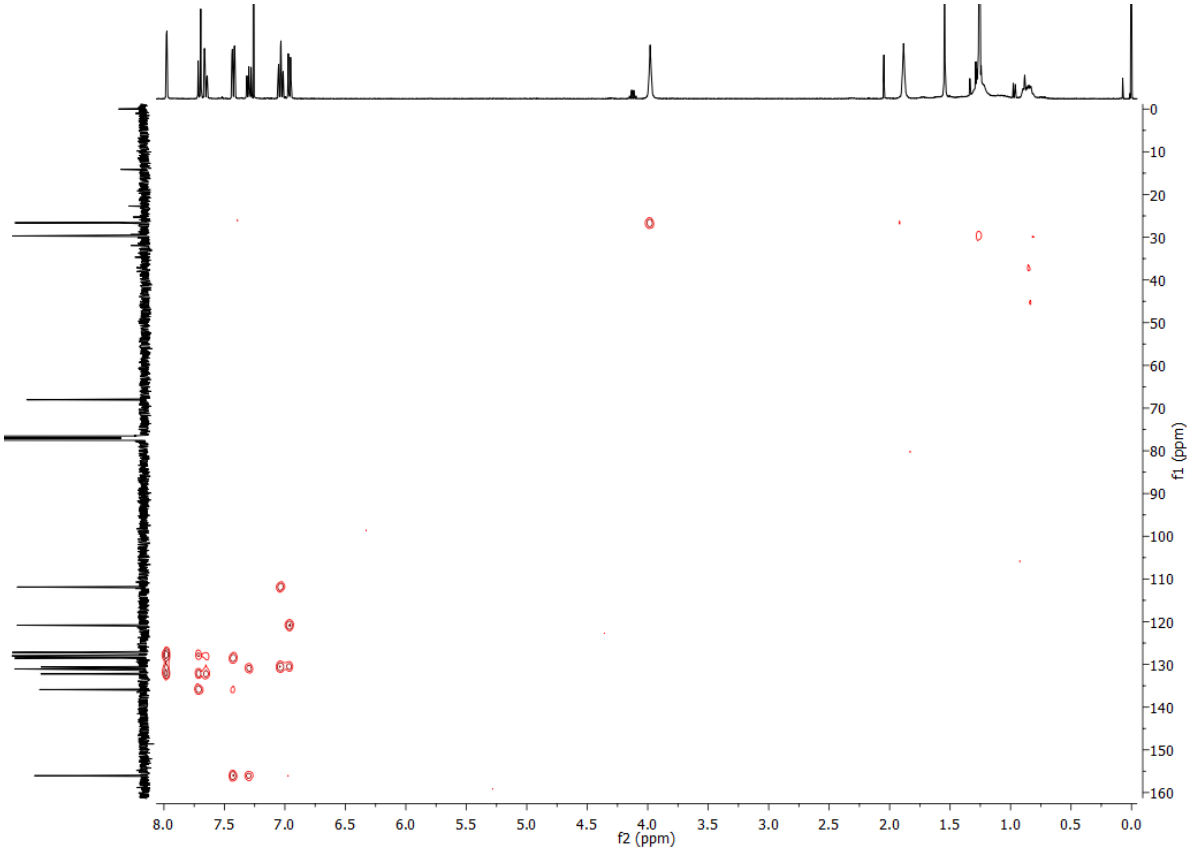

Figure S64. HMBC NMR of **Cyc-C4** in $CDCl_3$ at 298 K.

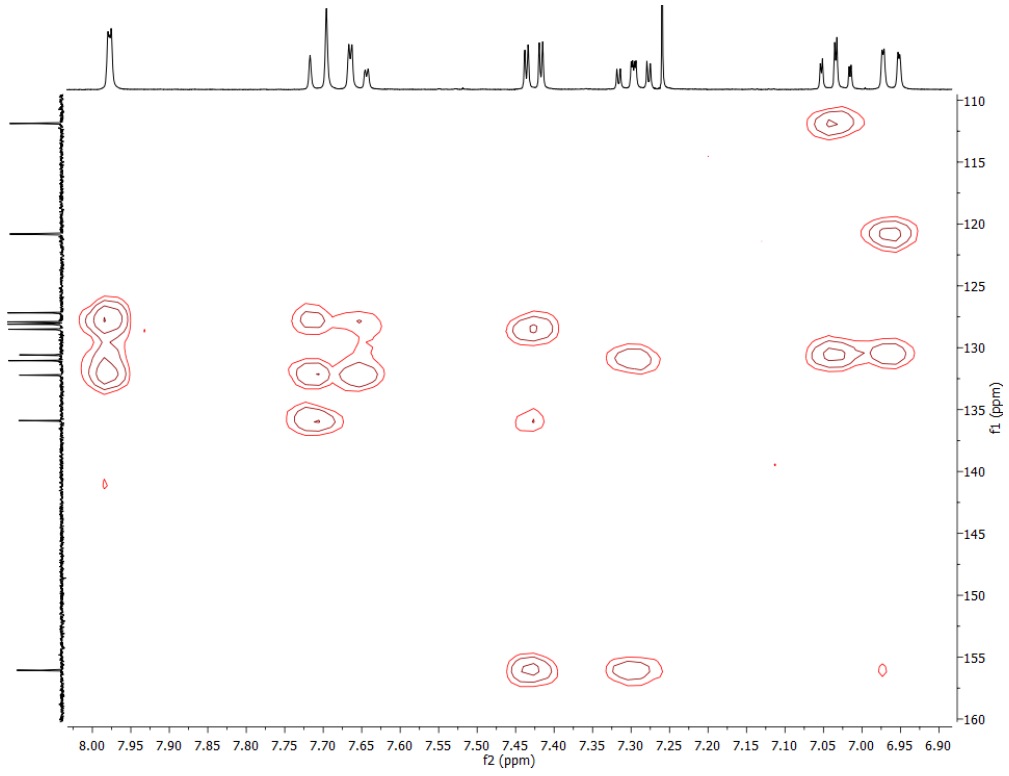

Figure S65. HMBC NMR of **Cyc-C4** in $CDCl_3$ at 298 K. Expansion of the aromatic region.

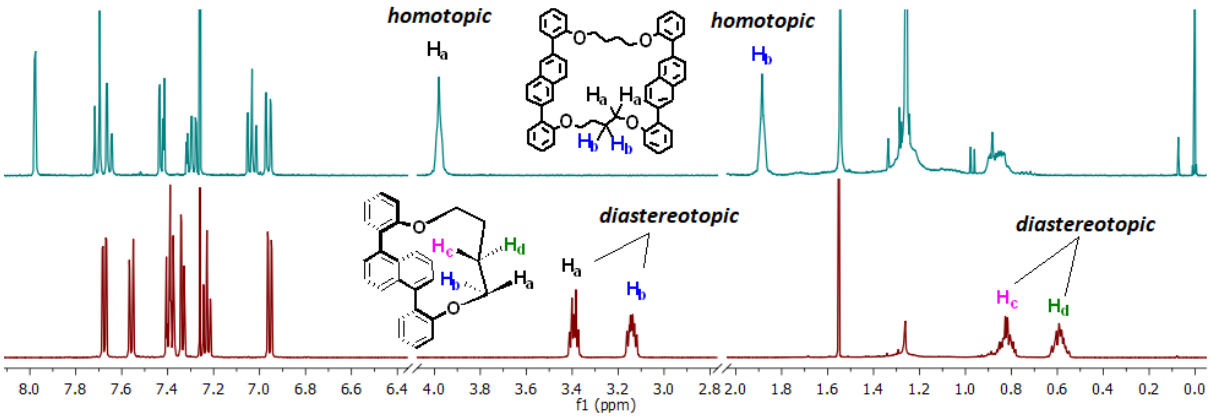

Figure S66. ^{1}H NMR comparison between intermolecular tethering and intramolecular tethering. The diastereotopic protons in the alkyl tether in **Nap-C4** (denoted as H_a and H_b) vs. the homotopic protons in the alkyl tether of **Cyc-C4**.

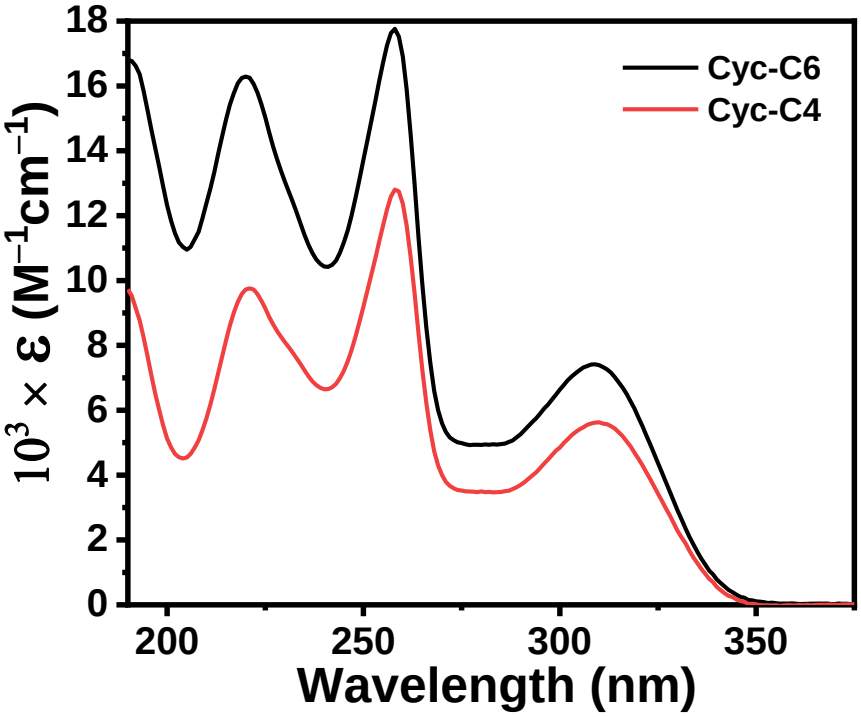

Figure S66. UV-Vis absorption spectra of Cyc-C6 (black) and Cyc-C4 in acetonitrile.

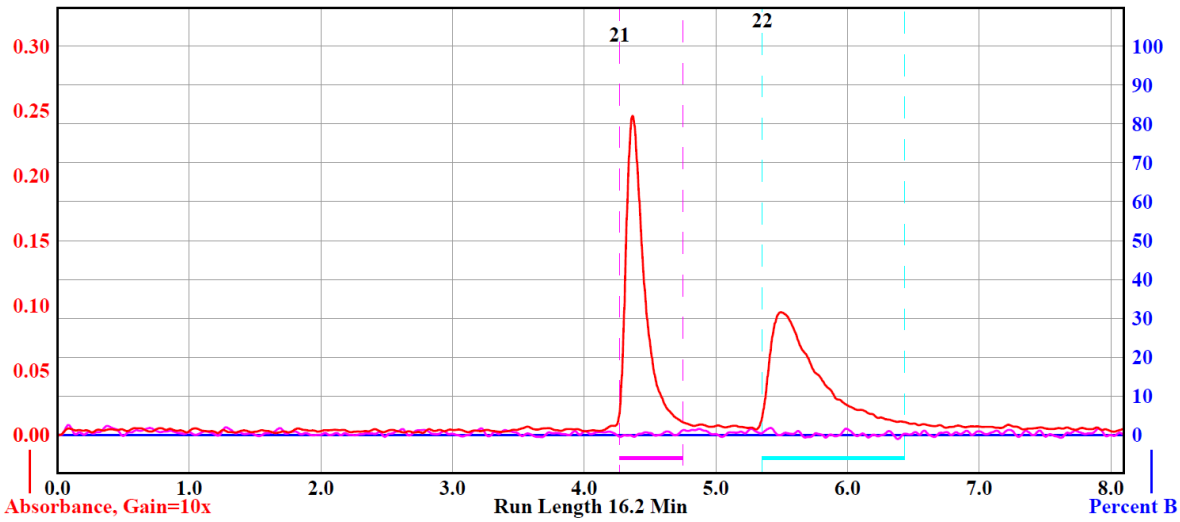

Figure S678. HPLC chromatogram for the enantio-separation of **Nap-C6**, separated on Chiralpak® IG semi-preparative column, with hexane/dichloromethane (85/15) as an eluent at room temperature.

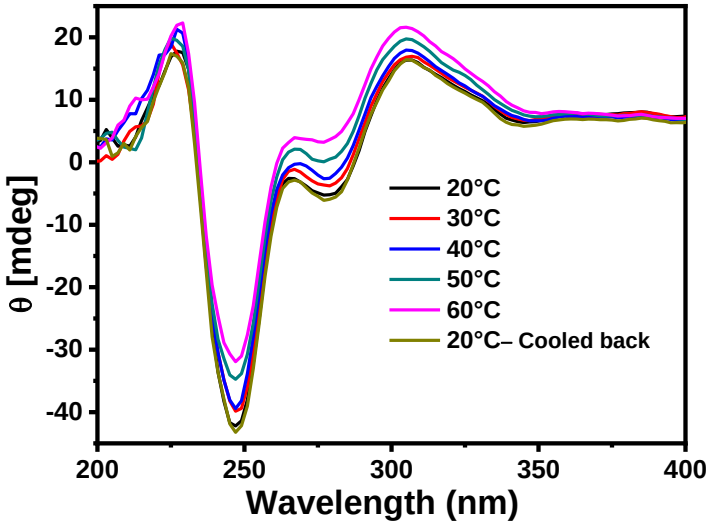

Figure S689. Variable temperature CD spectra of ***M*-Nap-C6** in acetonitrile.

S2 Computational details

All calculations were carried out using the Gaussian 09 program applying density functional theory (DFT). All molecules were optimized using a hybrid density functional[1] and Becke's three-parameter exchange functional combined with the LYP correlation functional (B3LYP) and with the 6-31G(d) basis set (B3LYP/6-31G(d)).[2] Theoretical UV-vis absorption spectra were obtained by TD-DFT calculation on these model structures using the 6-31G(d) basis set with CAM-B3LYP correlation function.[3]

S2.1 Cartesian coordinates of P-Nap-Cn calculated at the B3LYP/6-31G(d) level.

***P*-Nap-C4**

Standard orientation:

Center Number	Atomic Number	Atomic Type	Coordinates (Angstroms) X	Y	Z
1	6	0	-1.483701	-1.234815	2.048515
2	6	0	-0.159403	-1.381082	2.522591
3	6	0	-1.749174	-1.125102	0.696074
4	6	0	0.897298	-1.332670	1.643884
5	6	0	0.672271	-1.243931	0.243804
6	6	0	-0.672282	-1.243951	-0.243633
7	6	0	-0.897312	-1.332833	-1.643703
8	6	0	0.159389	-1.381354	-2.522406
9	6	0	1.483689	-1.235055	-2.048346
10	6	0	1.749165	-1.125193	-0.695917
11	1	0	-0.020918	-1.473986	-3.590096
12	1	0	2.301817	-1.148077	-2.758691
13	6	0	-3.115078	-0.722568	0.256915
14	6	0	-4.249057	-1.506496	0.505132
15	6	0	-3.298152	0.553234	-0.324961
16	6	0	-5.530443	-1.047189	0.195054
17	1	0	-4.115759	-2.488105	0.952422

18	6	0	-4.580123	1.016250	-0.631503
19	6	0	-5.694824	0.217774	-0.369907
20	1	0	-6.394496	-1.674994	0.394104
21	1	0	-4.692249	1.998102	-1.082748
22	1	0	-6.688459	0.583575	-0.615014
23	6	0	3.115071	-0.722613	-0.256809
24	6	0	3.298157	0.553271	0.324886
25	6	0	4.249046	-1.506576	-0.504934
26	6	0	4.580134	1.016327	0.631345
27	6	0	5.530437	-1.047231	-0.194934
28	6	0	5.694828	0.217810	0.369848
29	1	0	4.692270	1.998243	1.082448
30	1	0	6.394486	-1.675066	-0.393908
31	1	0	6.688468	0.583644	0.614890
32	8	0	-2.185327	1.306397	-0.613892
33	8	0	2.185336	1.306474	0.613714
34	1	0	-2.301829	-1.147755	2.758849
35	1	0	0.020902	-1.473603	3.590292
36	1	0	1.918103	-1.368394	2.010656
37	1	0	-1.918117	-1.368583	-2.010470
38	1	0	4.115740	-2.488246	-0.952091
39	6	0	1.966690	2.530952	-0.109343
40	1	0	2.643354	2.575799	-0.971209
41	1	0	2.202816	3.377324	0.552189
42	6	0	0.510100	2.595181	-0.574048
43	1	0	0.316044	1.744096	-1.234824
44	1	0	0.391108	3.507792	-1.177301
45	6	0	-0.510078	2.595237	0.573723
46	1	0	-0.316016	1.744223	1.234589
47	1	0	-0.391089	3.507911	1.176880
48	6	0	-1.966669	2.530952	0.109031
49	1	0	-2.643328	2.575895	0.970896
50	1	0	-2.202800	3.377252	-0.552591

P-Nap-C6

Standard orientation:

Center Number	Atomic Number	Atomic Type	Coordinates (Angstroms) X	Y	Z
1	6	0	-1.281200	-1.199847	-2.161352
2	6	0	0.073185	-1.220248	-2.564316
3	6	0	-1.629048	-1.259352	-0.825622
4	6	0	1.075903	-1.256734	-1.624060
5	6	0	0.770922	-1.334848	-0.237994
6	6	0	-0.602337	-1.391522	0.167130
7	6	0	-0.903923	-1.576727	1.543933
8	6	0	0.101772	-1.688146	2.475027
9	6	0	1.454529	-1.552108	2.086076
10	6	0	1.798031	-1.352385	0.763870
11	1	0	-0.140183	-1.849133	3.522402
12	1	0	2.235768	-1.565756	2.841439
13	6	0	-3.063352	-1.118841	-0.435901
14	6	0	-3.992310	-2.136450	-0.661760
15	6	0	-3.517698	0.097723	0.127602
16	6	0	-5.342322	-1.980276	-0.332483
17	1	0	-3.642024	-3.067880	-1.098845
18	6	0	-4.866648	0.259381	0.461436
19	6	0	-5.770874	-0.782041	0.230553
20	1	0	-6.045415	-2.788023	-0.513728
21	1	0	-5.220762	1.188743	0.892588
22	1	0	-6.816184	-0.643342	0.494324
23	6	0	3.214788	-1.058937	0.395484
24	6	0	3.565944	0.270281	0.055789
25	6	0	4.214283	-2.032489	0.398016
26	6	0	4.879970	0.586373	-0.301327

27	6	0	5.534390	-1.721017	0.054701
28	6	0	5.857463	-0.414326	-0.299611
29	1	0	5.149117	1.601479	-0.571633
30	1	0	6.295960	-2.495400	0.058356
31	1	0	6.877038	-0.158751	-0.576520
32	8	0	-2.565605	1.061947	0.297397
33	8	0	2.546699	1.172278	0.128273
34	1	0	-2.064039	-1.104029	-2.908996
35	1	0	0.318152	-1.178992	-3.622471
36	6	0	2.745549	2.526052	-0.267224
37	1	0	3.012463	2.567265	-1.334336
38	1	0	3.571662	2.969889	0.307070
39	1	0	2.116280	-1.240219	-1.932116
40	1	0	-1.943311	-1.644725	1.848672
41	1	0	3.945331	-3.051834	0.662654
42	6	0	1.446548	3.279267	0.007181
43	1	0	1.621910	4.340034	-0.223603
44	1	0	1.245188	3.222295	1.084736
45	6	0	-2.938920	2.329540	0.831878
46	1	0	-3.365699	2.199677	1.837283
47	1	0	-3.709415	2.788161	0.193574
48	6	0	-1.065495	3.527719	-0.488587
49	1	0	-0.871882	4.606579	-0.565939
50	1	0	-1.795353	3.296136	-1.274781
51	6	0	0.238495	2.766204	-0.791530
52	1	0	0.091701	1.699563	-0.596550
53	1	0	0.462793	2.860345	-1.863661
54	6	0	-1.698834	3.215757	0.891572
55	1	0	-2.004195	4.144608	1.390543
56	1	0	-0.966531	2.737511	1.553286

S2.2 Excitation energies and oscillator strengths of Nap-C4

Excited State 1: Singlet-A 4.3352 eV 285.99 nm f=0.3077 <S**2>=0.000

97 -> 98 0.67693

Excited State 7: Singlet-A 5.6276 eV 220.31 nm f=0.2976 <S**2>=0.000

92 -> 98 -0.12420
93 ->100 -0.15147
94 -> 98 0.12291
94 -> 99 -0.14287
95 ->101 0.14194
96 -> 98 0.26971
97 -> 99 0.35136
97 ->102 0.39478
97 ->103 -0.12396

Excited State 9: Singlet-A 5.9649 eV 207.85 nm f=0.3681 <S**2>=0.000

92 -> 98 0.18442
94 -> 98 -0.31108
95 ->100 -0.10619
96 -> 98 -0.16366
97 -> 99 -0.26321
97 ->102 0.33766
97 ->103 -0.29359

Excited State 16: Singlet-A 6.2950 eV 196.96 nm f=0.2927 <S**2>=0.000

92 -> 98 0.16890
94 -> 98 0.12686
94 ->103 0.17381
95 ->101 0.14449
96 -> 99 0.46406
97 ->102 -0.13857
97 ->103 -0.32195

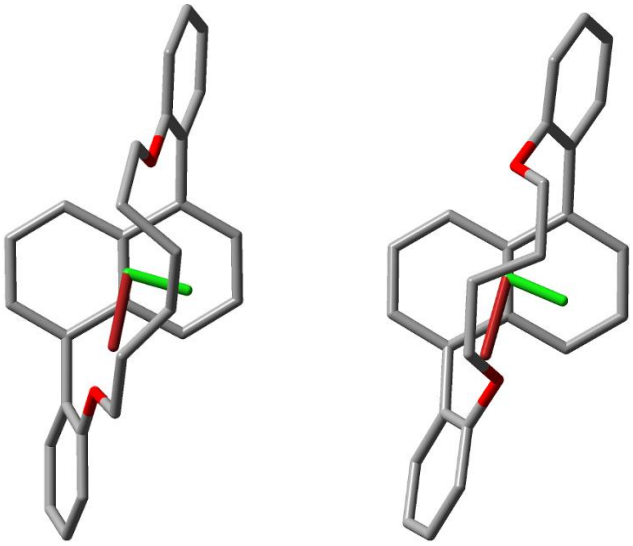

Figure S70. Electric (μ_e, red) and magnetic (μ_m, green) transition dipole moments for the lowest energy transition in **Nap-C6** (left) and **Nap-C4** (right).

Table S1. Calculated values for electric and magnetic transition dipole moment, rotatory strengths for **Nap-Cn**.

	μ_e			μ_m			Rotatory strength (R_{vel}) in cgs (10^{-40}erg-esu-cm-G^{-1}	Angle between μ_e and μ_m
	X	Y	Z	X	Y	Z		
Nap-C6	-1.6024	0.0534	0.1126	-0.0216	0.0287	1.3153	45.4	95.0
Nap-C4	1.6961	0.0000	-0.1407	0.0596	0.0000	1.2636	71.6	97.9

1. Parr, R. G.; Yang, W., *Density-functional theory of atoms and molecules*. ed.; Oxford University Press ; Clarendon Press: New York, Oxford England, **1989**.

2. Lee, C.; Yang, W.; Parr, R. G. *Phys. Rev. B* **1988,** 37, 785-789.

3. Gaussian 09, Revision D.01, Frisch, M. J.; Trucks, G. W.; Schlegel, H. B.; Scuseria, G. E.; Robb, M. A.; Cheeseman, J. R.; Scalmani, G.; Barone, V.; Mennucci, B.; Petersson, G. A.; Nakatsuji, H.; Caricato, M.; Li, X.; Hratchian, H. P.; Izmaylov, A. F.; Bloino, J.; Zheng, G.; Sonnenberg, J. L.; Hada, M.; Ehara, M.; Toyota, K.; Fukuda, R.; Hasegawa, J.; Ishida, M.; Nakajima, T.; Honda, Y.; Kitao, O.; Nakai, H.; Vreven, T.; Montgomery, Jr., J. A.; Peralta, J. E.; Ogliaro, F.; Bearpark, M.; Heyd, J. J.; Brothers, E.; Kudin, K. N.; Staroverov, V. N.; Keith, T.; Kobayashi, R.; Normand, J.; Raghavachari, K.; Rendell, A.; Burant, J. C.; Iyengar, S. S.; Tomasi, J.; Cossi, M.; Rega, N.; Millam, J. M.; Klene, M.; Knox, J. E.; Cross, J. B.; Bakken, V.; Adamo, C.; Jaramillo, J.; Gomperts, R.; Stratmann, R. E.; Yazyev, O.; Austin, A. J.; Cammi, R.; Pomelli, C.; Ochterski, J. W.; Martin, R. L.; Morokuma, K.; Zakrzewski, V. G.; Voth, G. A.; Salvador, P.; Dannenberg, J. J.; Dapprich, S.; Daniels, A. D.; Farkas, O.; Foresman, J. B.; Ortiz, J. V.; Cioslowski, J. and D. J. Fox, Gaussian, Inc., Wallingford CT, **2013**.